P10 Granular Filtration in a Fluidized Bed

J.S. Mei, P.C. Yue, and J.S. Halow
Morgantown Energy Technology Center

ABSTRACT

Successful development of advanced coal-fired power conversion systems often require reliable and efficient cleanup devices which can remove particulate and gaseous pollutants from high-temperature high-pressure gas streams. A novel filtration concept for particulate cleanup has been developed at the Morgantown Energy Technology Center (METC) of the U. S. Department of Energy. The filtration system consists of a fine metal screen filter immersed in a fluidized bed of granular material. As the gas stream passes through the fluidized bed, a layer of the bed granular material is entrained and deposited at the screen surface. This material provides a natural granular filter to separate fine particles from the gas stream passing through the bed. Since the filtering media is the granular material supplied by the fluidized bed, the filter is not subjected to blinding like candle filters. Because only the in-flowing gas, not fine particle cohesive forces, maintains the granular layer at the screen surface, once the thickness and permeability of the granular layer is stabilized, it remains unchange as long as the in-flowing gas flow rate remains constant. The weight of the particles and the turbulent nature of the fluidized bed limits the thickness of the granular layer on the filter leading to a self-cleaning attribute of the filter. Batch mode filtration performance of the filter was first reported at the Ninth Annual Coal-Fueled Heat Engines, Advanced Pressurized Fluidized-Bed Combustion, and Gas Stream Cleanup Systems Contractors Review Meeting. This poster paper presents work since then on a continuous filtration system.

The continuous filtration testing system consisted of a filter, a two-dimensional fluidized-bed, a continuous powder feeder, a laser-based in-line particle counting, sizing, and velocimeter (PCSV), and a continuous solids feeding/bed material withdrawal system. The two dimensional, transparent fluidized-bed allowed clear observation of the general fluidized state of the granular material and the conditions under which fines are captured by the granular layer. A series of experiments were conducted over various ranges of operating conditions with two different bed materials: a 30x270 mesh acrylic powder with particle density of 1.1 gm/cc and a 40x270 mesh Millwood sand which has particle density of 2.5 gm/cc. During the experiments, fine sand (less than 100 micron) was fed continuously to the bed through the powder feeder at a constant rate of 3.8 gm/min (0.5 lb/hr). Bed material and captured fine particles were withdrawn continuously through an overflow tube. In order to maintain a constant bed level, makeup bed material was also fed continuously through an non-mechanical valve to the bottom of the fluidized bed. Performance of this granular filtration system was measured by the PCSV at downstream of the filter.

High filtration performance was measured when lower density powder was used as bed material. Collection efficiencies over 99 % were obtained with this bed material in a continuous flow mode. Low filtration performance was experienced with heavier bed material. The low filtration performance with this material may be attributed to the failure of maintaining a sufficiently thick granular layer at the screen filter surface. Filtration performance as a function of particle size distribution and the pressure drop across the granular filter will also be discussed in this poster paper.

P11

Dust Cake Behavior in Filters With High Surface Area to Volume Ratios

Douglas Straub
Ta-Kuan Chiang
Richard A. Dennis
Morgantown Energy Technology Center

INTRODUCTION

High-temperature particulate control devices are an integral part of advanced coal-fired power systems. By efficiently removing minute particles from high-temperature gas streams, environmentally clean and efficient power systems can be realized. In recent years, economic incentives have prompted developers of high-temperature and high-pressure (HTHP) particulate filtration systems to pursue filter element designs with more filter surface area for a given volume. Although higher surface-to-volume (SV) ratio filter designs are driven by economic incentives, physical constraints and the fundamental behavior of dust cake formation and removal will limit the maximum SV ratio.

In an attempt to improve the understanding of dust cake behavior in a well controlled environment, a two-dimensional cold flow filter module is being tested. This filter module can be used to investigate dust cake formation, removal, and re-entrainment over a range of operating conditions. Some of the operating conditions investigated include filter spacing (3.2 and 6.4 cm), filter length (51 and 102 cm), face velocity (160 to 460 cm/min), particle loading (10,000 to 40,000 ppm), and the physical properties of the particulate media.

Preliminary results suggest that the cohesive strength of the particulate media has a strong influence on how the dust cake is removed during reverse pulse cleaning. Furthermore, the properties of the particulate media play an important role in forming non-uniform dust cakes. In the following paragraphs, the experimental apparatus, preliminary results, and future plans will be discussed.

EXPERIMENTAL APPARATUS

In these tests, compressed air was used as a carrier gas for the particulate media studied. During the test, the air flow rate and pressure drop across the filter module were monitored by Rosemount (Model 3051) differential pressure transmitters. Flyash was injected using a K-Tron (Model #T20-90-048-F1) twin screw dust feeder. The filter surfaces were constructed from Grade 5 sintered stainless steel. This 1.6-mm thick filter slab had a pore size distribution in the 50 to 100 micrometer range. The air and particulate flow entered the filter plenum at the bottom of the filter module, and flowed upward into a rectangular channel formed by the two filter surfaces and two optically clear Lexan windows. (See Figure 1.)

In order to quantify dust cake thickness variations and determine dust cake permeabilities, an optical device was developed to measure the dust cake thickness in-situ. (See Figure 2.) This device monitored the cake thickness over the entire length of the filter.

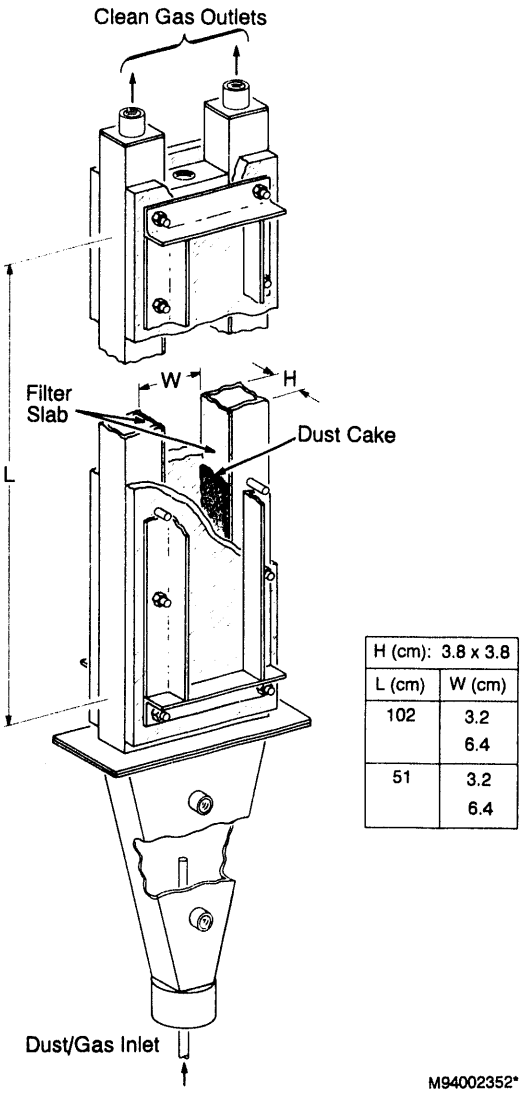

H (cm): 3.8 x 3.8	
L (cm)	W (cm)
102	3.2
	6.4
51	3.2
	6.4

Figure 1. Schematic of the Filter Test Module

The following three flyash materials have been proposed for study:

Sample 1: Pressurized Fluidized Bed Combustor (Tidd) flyash, sample taken December 1992

Sample 2: Pressurized Fluidized Bed Combustor (Tidd) flyash, sample taken February 1994

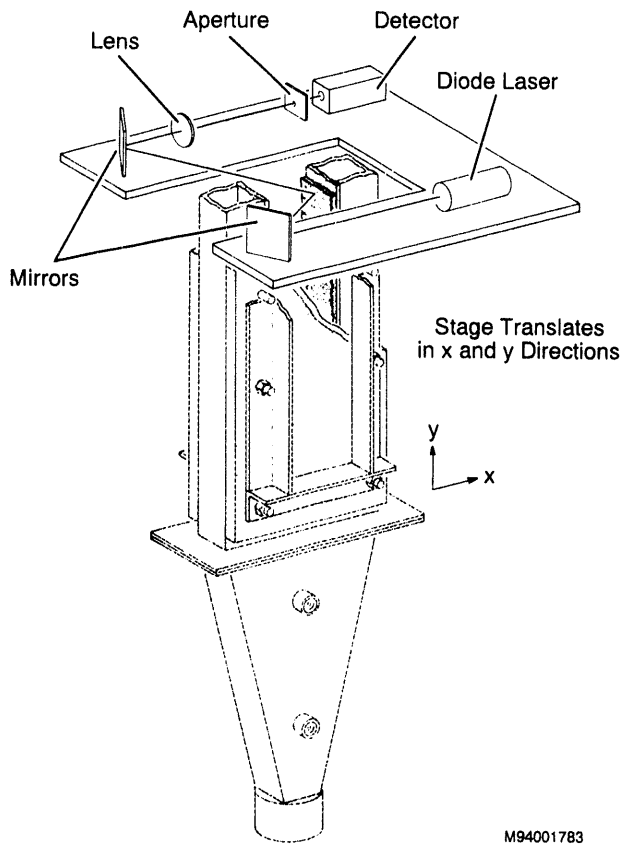

Figure 2. Schematic of the Dust Cake Measurement Device

Sample 3: Pulverized Coal Boiler (Ft. Martin) flyash

The major differences between Sample 1 and Sample 2 are a result of process modifications made at the Pressurized Fluidized-Bed Combustor (PFBC) plant facility. These modifications included spoiling the efficiency of a cyclone located upstream of the filter vessel, and injecting tempering air to lower the operating temperature in the filter vessel. The preliminary results presented in this paper will concentrate on Samples 1 and 3. Testing of Sample 2 will be completed in the future.

RESULTS AND DISCUSSION

The following discussion will address the particulate media characterization, dust cake formation, and dust cake removal data that have been collected at this time.

Particulate Media Characterization

Prior to testing, the particle size distributions were characterized by a Coulter Scientific Multi-sizer II. The mean particle diameters on a volume and population basis are shown in Table 1. The particle density was characterized by a Micromeritics Accu-Pic 1330 helium pycnometer. These results are also shown in Table 1.

In addition to the standard particle size and density analyses, Samples 1 and 2 were analyzed in greater detail. The bulk uncompacted fracture strengths were measured for Samples 1 and 2 as a function of temperature. (See Figure 3.) These samples were heated in a nitrogen environment, and the voidages of both samples were maintained at 86 percent. The theoretical relationship between fracture strength of bulk powders and the properties of its constituent particles can be expressed as follows (Molerus 1975):

$$\sigma_f = \frac{(1-\varepsilon)}{\pi} K \frac{H}{d^2} \quad , \qquad (1)$$

where

σ_f = Fracture strength, (Pa),
ε = Bulk powder porosity,
K = Co-ordination number (varies in the range of 6 to 16 for a uniform size distribution),
H = Isotropic contact force between particles, (N), and
d = Particle diameter, (m).

Although this expression has a strong dependence upon particle size, the Coulter Counter and the dry aerodynamic particle size analyses indicated that a factor of 30 difference in fracture strength could not be explained by differences in particle size alone. Thermogravimetric analyses were conducted to determine if these two samples exhibited significantly different chemical behavior. (See Figures 4 and 5.) Although these analyses showed similar trends, Sample 1 demonstrated a faster rate of weight loss around 900°C (1650°F). It is suspected that this weight loss is due to the decomposition of $CaMg_3(SO_4)_4$, and the faster rate observed for Sample 1 may be indicative of a higher concentration. At this time, it is not clear how $CaMg_3(SO_4)_4$ affects the fracture strength, but testing is planned to answer this question.

Table 1. Particulate Media Characteristics

Sample Number	Description	Mean Size Volume % (micrometer)	Mean Size Number % (micrometer)	Particle Density (g/cc)
1	PFBC Ash - Tidd (Sample taken 12/92)	4.63	2.50	2.84
2	PFBC Ash - Tidd (Sample taken 2/94)	5.63	2.55	2.78
3	PC Boiler Ash - Ft. Martin	67.53	20.81	2.74

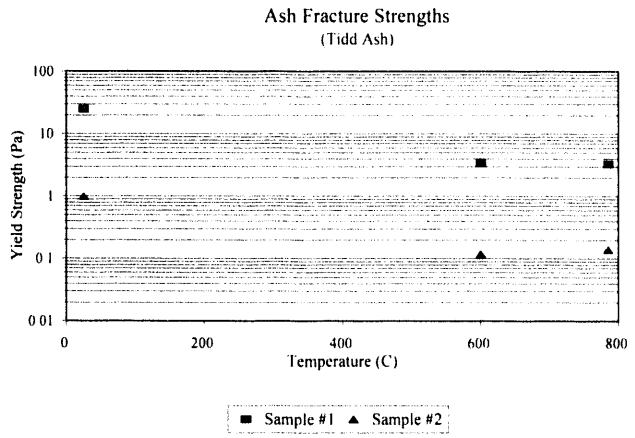

Figure 3. Fracture Strength of Two Pressurized Fluidized Bed Combustor Flyash Samples as a Function of Temperature

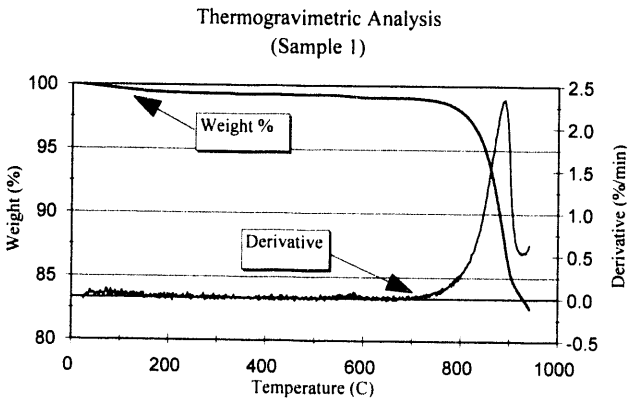

Figure 4. Thermogravimetric Analysis or Pressurized Fluidized Bed Combustor Flyash - Sample 1

Dust Cake Formation Behavior

The air and particulate were injected from the bottom of the plenum, upward toward the filter channel. The operating conditions investigated are shown in Table 2. It should be noted that the filter module with the 6.4-cm spacing was blinded at a face velocity of 458 cm/min. At this high face velocity, particles penetrated the surface of the porous metal surface and became trapped within the filter wall. As a result, the filter permeability decreased, and backflush cleaning was no longer effective. The filter module with the 6.4-cm spacing was blinded very early in the test plan, so the effect of filter aspect ratio has not been thoroughly investigated at this time.

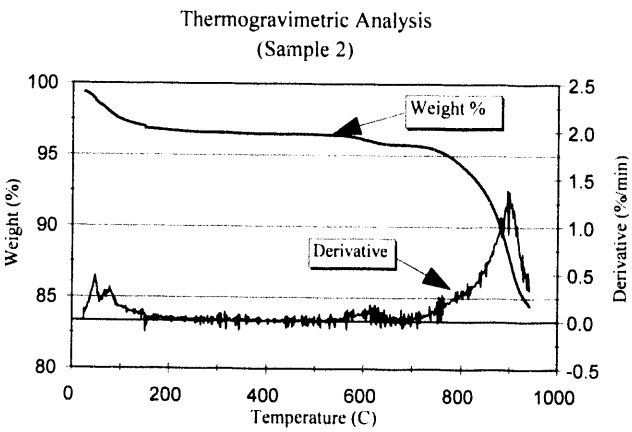

Figure 5. Thermogravimetric Analysis or Pressurized Fluidized Bed Combustor Flyash - Sample 2

For Sample 1, dust cake thicknesses were uniform for all of the operating conditions studied. However, when Sample 3 was investigated under the same operating conditions, distinct features formed along the top half of the filter surfaces. The length of these irregularly shaped mounds ranged from a few millimeters to roughly 50 mm. The thicknesses and the widths were in the 1 to 7 mm range. Along one filter surface, these features were periodically spaced every 35 to 40 mm. This filter surface had a small depression (roughly 25 to 40 mm in diameter and roughly 5 mm deep) located near the middle of the filter surface length. This depression was formed during assembly of the filter module, and may have been introducing turbulent effects into the flow. The mound-like features seemed to be more distinct at higher face velocities which also suggests that these features are dependent upon turbulent effects.

Table 2: Operating Conditions Investigated

Filter Aspect Ratio (length/filter spacing)	Face Velocity (cm/min)	Particle Loading (ppm)
32	168	10,000
32	168	40,000
32	229	10,000
32	229	40,000
16	229	10,000
8	458[1]	10,000

[1] This face velocity blinded the filter module with a 6.4 cm spacing.

These irregular formations were observed with Sample 3, and not with Sample 1. A potential explanation for this difference may be due to the significantly larger particle size distribution for Sample 3, and the fact that the gas momentum in the vertical direction is depleted along the length of the filter. Noting that the largest particles in Sample 3 are in the 100 to 200 micrometer range, at some point along the length of the filter, the velocity falls below the terminal velocity for these particles. Since the body forces on these large particles are more dominant than the drag forces pulling them to the filter surface, the particles fall toward the inlet of the filter module. At some point near the inlet, the vertical velocity component is large enough to re-entrain these particles. This behavior causes the particles to circulate, and is readily observed over an area of 35 to 50 cm of the filter length. This particle motion introduces more turbulence toward the top of the filter module, where the irregular dust cake features are observed. It is important to note that these features are easily removed during reverse pulse cleaning.

Dust Cake Removal Behavior

The behavior of Sample 1 and Sample 3 during pulse cleaning was significantly different. Under the same operating conditions, Sample 1 exhibited "patchy" or incomplete cleaning, whereas Sample 3 cleaned uniformly. The tensile strength of Sample 3 has not been measured, but Sample 1 seems significantly more cohesive.

When the dust cake removal is incomplete, it has been observed that subsequent cleaning pulse cycles do not remove the dust cake from the areas which were previously not cleaned. Although these "patches" have significantly lower permeabilities than the clean areas, the dust cake continues to form on these patches at a slow rate. Over time, these "patches" may lead to significant ash build-up and become nucleation sites for ash bridges. Qualitatively speaking, these "patches" seem to be more prominant near the top of the filter surface, but more data is necessary to substantiate this observation.

Although these results are preliminary, they emphasize the importance of dust cake properties on cleaning behavior, as well as behavior during dust cake formation. A thorough understanding of the relationship between particluate media properties and cleaning behavior of a particular media will lead to improved filter element designs and cleaning techniques.

FUTURE WORK

Plans for this project are as follows:

- Complete testing for Sample 2.
- Measure fracture strength of Sample 1 and Sample 3 at 925°C, to determine if the weight loss observed in the thermogravimetric analyses is responsible for increasing the ash cohesive strength. If these fracture strength measurements are significantly different than the measurements made at a slightly lower temperature, a thorough chemical analysis will be conducted.
- Utilize fast response instrumentation to characterize cleaning parameters.
- Improve existing module design to allow better quantification of incomplete cleaning.
- Investigate the feasibility of new filter designs and cleaning techniques.

ACKNOWLEDGEMENTS

We would like to gratefully acknowledge the diligent efforts of Mr. Rick Williams (EG&G) for his assistance in maintaining and operating this project. We would also like to thank Dr. Steven Woodruff (METC) for his expertise and efforts to develop our dust cake measurement device. Dr. H. O. Kono (West Virginia University) has played a key role in analyzing the fracture strengths of the particulate media used in these tests, and we would like to gratefully acknowledge his expertise and contributions.

REFERENCES

Molerus, O., "Theory of Yield of Cohesive Powders," *Powder Technology,* **12**, (1975), 259-275.

P12 Computer Simulations of IGCC/PFBC Components

Edward. J. Boyle, Thomas J. O'Brien, and Lawrence J. Shadle
Morgantown Energy Technology Center

Madhava Syamlal and Suresh Venkatesan
EG&G Technical Services of West Virginia

ABSTRACT

This modeling activity has provided numerical simulations and graphical visualizations of several IGCC and PFBC components. Specifically, the PyGas component of the Gasification Product Improvement Facility (GPIF) and the Industrial Filter and Pump (IFP), Tidd, and Karhula High Temperature, High Pressure (HTHP) filter unit were simulated. These calculations couple the complex physical phenomenon which affect the behavior of these units, such as, fluid dynamics, solid motion, heat transfer, and chemistry. Since all of these factors interact in a very nonlinear fashion, a complex computer code, based on multi-phase hydrodynamics is required in order to perform the simulations. The MFIX code, developed at METC, and the Fluent code, commercially available from Fluent Inc., were used for these simulations.

The GPIF contains is a novel coal gasification unit. It consists of a central "riser" in which caking coal is devolatilized, a free-board region, in which tar is combusted, and a concentric fixed-bed annular region, in which most of the gasification is completed. Air and coal is fed at the bottom of the riser. A shallow bed of coal and ash forms around the inlet jet. Solids strands of matter are lifted through the riser and overflow into the surrounding fixed-bed. Air is introduced from the top, with a radial divergence, to combust the tar produced during coal pyrolysis in the riser. A hot, annular recirculation region is predicted around this inlet, against the top dome of the vessel. The simulations predict that it will not be possible to sustain a co-flow gasification region. Gas flow from the riser section flows directly below the baffle and into the exit stream. This region shows large fluctuations in particle and gas velocity. Gas flow from below the grate supporting the fixed bed establishes a hot combustion front near the surface of the grate.

Several advanced power systems incorporate HTHP clean-up devices based on ceramic candle filter technology. The Fluent code was used to simulate gas/solid flow in the vessel housing these filters. The simulation of the Karhula design showed that the gas flow from the inlet was splitting on a baffle plate just inside the vessel, circulating down and around between the vessel and an inner shroud, and splashing over the inner shroud 180° from the inlet. This flow was so intense that it was entraining gas, up and out, over the shroud just behind the baffle.

The net effect was that the flow field on the candles themselves was very uneven. Various baffle designs were explored in order to distribute the flow more evenly. Because the inlet was located near the middle of the pressure vessel in the Tidd configuration, the flow pattern in that device was not nearly as complex. Both of these facilities were simulated using the 3-D capabilities of the Fluent code.

A series of simulations were performed in support of the IFP design. Because of the high degree of symmetry in this design, a series of simulations of different design options were performed in 2-D, cylindrical coordinates since this was less demanding computationally. The dimensions of the vessel were accurately represented, but the candles were idealized to a concentric filter ring with the same horizontal "footprint" as the actual array of 78 candles. In order to investigate the extent of flow between the candles, a 30° sector was simulated in 3-D using periodic boundary conditions. Since this calculation still used cylindrical coordinates, the individual candles were resolved so that their horizontal cross-sections were truncated pie shapes, rather than circular. However, their horizontal locations and cross-sections were preserved.

P13 Scaling of Pressurized Fluidized Beds

CONTRACT INFORMATION

Cooperative Agreement	DE-FC21-92MC29264
Contractor	Massachusetts Institute of Technology 77 Massachusetts Avenue Cambridge, MA 02139 (617) 253-2233
Contractor Project Manager	Susan Guralnik
Principal Investigator	Leon R. Glicksman
METC Project Manager	Peter Botros
Period of Performance	October 1, 1992 to September 31, 1995

FY 1994 Program Schedule

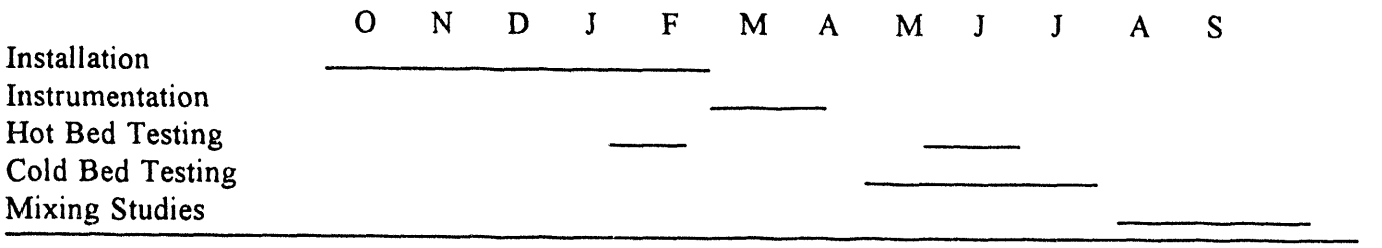

OBJECTIVES

This project has two primary objectives. The first is to verify a set of hydrodynamic scaling relationships for commercial pressurized fluidized bed combustors (PFBC). The second objective is to investigate solids mixing in pressurized bubbling fluidized beds.

American Electric Power's (AEP) Tidd combined-cycle demonstration plant will provide time-varying pressure drop data to serve as the basis for the scaling verification. The verification will involve demonstrating that a properly scaled cold model and the Tidd PFBC exhibit hydrodynamically similar behavior.

An important issue in PFBC design is the spacing of fuel feed ports. The feed spacing is dictated by the fuel distribution and the mixing characteristics within the bed. After completing the scaling verification, the cold model will be

used to study the mixing characteristics of PFBCs. A thermal tracer technique will be utilized to study mixing both near the fuel feed region and in the far field. The results will allow the coal feed and distributor to be designed for optimal mixing.

BACKGROUND INFORMATION

Hydrodynamic scaling

One of the most difficult problems facing a fluidized bed designer is to determine how bed size and operating parameters affect bed performance. This is particularly true when a large combustor is to be designed based on pilot plant experience. It is also critical in the operation or modification of an existing fluidized bed combustor. Research has been done to show that a cold model, designed using the proper hydrodynamic scaling parameters, closely simulates the hydrodynamic behavior of fluidized bed combustors. Accurate room temperature simulations of fluidized bed combustors allow rapid, inexpensive tests to determine the effects of varying operating parameters and bed design on the hydrodynamics of the combustor.

One of the first systematic developments of the dimensionless scaling parameters which control the modeling of a fluidized bed was presented by Glicksman (1984, 1988). The scaling parameters were developed by nondimensionalizing Anderson and Jackson's (1967) equations of motion. The resulting parameters, which we will refer to as the full set of scaling parameters, are as follows:

$$\frac{\rho_f}{\rho_s} \quad \frac{u_o^2}{gD} \quad \frac{\rho_f u_o D}{\mu} \quad \frac{L}{D} \quad \frac{D}{d_p} \quad \phi_s \quad PSD \qquad (1)$$

A great deal of experimental work has been done to verify that when these dimensionless groups are matched between two fluidized beds they exhibit hydrodynamically similar behavior (e.g. for bubbling beds: Nicastro and Glicksman, 1984; Newby and Keairns, 1986; Roy and Davidson, 1989; Almstedt and Zakkay, 1990; and for circulating beds: Glicksman et al., 1991; Chang and Louge, 1992, and Glicksman et al., 1993.)

When the full set of scaling parameters is used, once the scale model fluidizing gas is specified the size of the model is fixed. For example, if air at atmospheric temperature and pressure is used in a cold model of an atmospheric fluidized bed combustor, the model's linear dimensions will be roughly 1/4 those of the hot bed (scale down by factor of four). For the case of pressurized fluidized beds operating at 10-12 atm, a cold model fluidized using ambient air will have approximately the same linear dimensions as the combustor. This makes scaling large combustors using the full set of scaling parameters less tractable. Therefore, it is desirable to look for simplifications to the full set of scaling parameters which will make it possible to choose the scale factor.

Glicksman et al. (1993) proposed a simplification to the full set of scaling parameters which allows the scale factor to be independently specified. The simplification is based on the fact that the number of dimensionless groups can be reduced if the fluid-particle drag is dominated by either viscous or inertial effects. In both the viscous and inertial limits, the scaling parameters reduce to:

$$\frac{\rho_f}{\rho_s} \quad \frac{u_o^2}{gD} \quad \frac{u_o}{u_{mf}} \quad \frac{L}{D} \quad \phi_s \quad PSD \qquad (2)$$

where the bed Reynolds number and the ratio of the reference bed dimension (D) to the particle

diameter (d_p) in the full set [Eqtn. (1)] have been replaced by the ratio of the gas superficial (u_o) and minimum fluidization velocities (u_{mf}). Since this simplified set of parameters holds exactly at both high and low particle Reynolds numbers, it is reasonable to expect it to be approximately valid throughout the range of particle Reynolds numbers. Equation (2) will be referred to as the simplified set of scaling parameters. Glicksman et al. (1993) experimentally verified the simplified set of scaling parameters for atmospheric circulating fluidized beds (CFB) by making hydrodynamic comparisons between three fluidized beds. Hot-bed data was taken from the 2.5 MW_t Studsvik CFB prototype. Scaling comparisons were made between the hot-bed, a 1/4 scale model of the Studsvik CFB based on the full set of scaling parameters, and a 1/16 scale model of the hot-bed based on the simplified set of scaling parameters. The solid fraction profiles of the three beds were found to agree well.

Solids mixing

A properly scaled cold model provides similar hydrodynamics to that of a hot combustor. Solids mixing in bubbling beds is due primarily to bubble characteristics such as bubble size and frequency, which induce mixing in bubble wakes, and to bubble eruptions at the bed surface. A cold scale model with similar hydrodynamics makes it possible to investigate solids mixing for a hot bed combustor.

Lateral and vertical solids mixing is critical in fluidized bed combustors. Adequate mixing is required to ensure high combustion efficiency, sulphur capture, and heat transfer. Solid mixing is typically investigated using tracer techniques. These techniques involve the injection of tracer particles into a fluidized bed and the tracking of their movement in some way. The tracer should have the same density, diameter, and sphericity as the bed material so that its movement will accurately characterize particle motion within the bed. For an ambient air fluidized cold model of a pressurized fluidized bed combustor, the solid density must be approximately 900 kg /m^3. This rules out the use of magnetic tracers or other high density materials. Also, due to the seemingly random behavior of fluidized beds, numerous experiments need to be conducted to characterize the average solids mixing characteristics of the bed. Therefore the technique should not produce an elevated background of the tracer particles which would make it impossible to distinguish between tracers from current and previous experiments. A thermal tracer technique was developed (Valenzuela and Glicksman, 1984) which satisfies these criterion. It has also recently been used to study lateral solids mixing in circulating fluidized beds (Westphalen, 1993). The thermal tracer technique involves the injection of heated bed material particles into the fluidized bed. The motion of the particles is tracked using an array of thermistor probes. This technique has the advantage that the bed material is used as the tracer ensuring that the hydrodynamics will be similar. The heated tracers lose their distinctive signature after some residence time in the bed thus not disturbing the overall background level of subsequent experiments.

PROJECT DESCRIPTION

Hydrodynamic scaling

Experiments will be carried out on the Tidd PFBC and on a cold scale model at MIT. For bubbling beds, important bed characteristics such as gas and solids mixing and heat transfer are a direct function of the bubble characteristics. Thus the experimental verification will be based on a comparison of bubble characteristics.

Time-resolved pressure differences between two vertically spaced static pressure taps give a good indication of the bubble behavior; the amplitude is proportional to the bubble size while the frequency of the fluctuations gives the frequency of bubbles passing between the probes. Comparisons of these quantities can be made by evaluating the probability density function (PDF) and power spectral density (PSD) of the time-varying pressure signal. By placing probes at several locations within the bed, the spatial variation of bubble characteristics can be obtained. Verification of the scaled model with the combustor will be obtained by comparing the PDF and PSD results in nondimensional form.

Solids mixing

After the cold model is verified, it will be used to study solids mixing. The thermal tracer technique will be used.

There are two important sources of mixing which have an impact on the required coal feed spacing. Close to the feed point, mixing is determined by the interaction of the injected fuel and water flow with the bed dynamics. In this region, the momentum of the injected mass and the feed point design may be important. As the material moves away from the feed point into the far field, vertical and lateral mixing of the fuel and volatiles will be determined by the bed dynamics.

To simulate near field mixing in the vicinity of the feed point, preliminary experiments will be carried out using solid tracer and air injected with the same scaled flow rate and momentum as the fuel/water stream. It may also be necessary to simulate the dynamics of the phase change of the water injected with the coal. This may be modeled using chilled liquid refrigerant.

The thermal tracer technique in conjunction with the cold scale model will make it possible to evaluate the effect of varying operating parameters and bed geometry on the solids mixing.

RESULTS

Scaling calculations

Table 1 lists the geometric and operating parameters which are needed to calculate the values of the simplified scaling parameters for the Tidd PFBC. The particle density (ρ_s) was determined by measuring the displacement of a known mass of the Tidd bed material (dolomite). The particle sphericity (ϕ_s) was determined by evaluating a digitized picture of the Tidd bed material using computer software to estimate its average apparent circularity. Chang and Louge (1992) found that the square of the apparent circularity provided a good estimate of the particle sphericity. The particle diameter was determined through sieve analysis, and the minimum fluidization velocity was predicted using an expression proposed by Grace (1982).

Table 1 also lists the parameters for a 1/4 scale cold model of the Tidd PFBC based on the simplified set of scaling parameters. The values in the table are those required to exactly match the scaling parameters. The fluidizing gas properties are those of ambient air.

Cold scale model

A quarter scale cold scale model of a section of the Tidd PFBC has been constructed based on the simplified set of scaling laws. The Tidd boiler enclosure (Kinsinger, 1990) is illustrated in Figure 1. The dashed lines represent the section of the Tidd combustor

Table 1. Comparison of Tidd PFBC and required cold model parameters

	Tidd PFBC	Cold Model (1/4 Scale)
T (°K)	1116	322
p (N/m^2)	$1.013x10^6$	$1.013x10^5$
μ (kg/m-s)	$4.5x10^{-5}$	$2.0x10^{-5}$
ρ_f (kg/m^3)	3.2	1.1
ρ_s (kg/m^3)	2513	875
ϕ_s	0.82	0.82
u_{mf} (m/s)	0.27	0.13
u_o (m/s)	0.91	0.45
D (m)	3.4	0.85
d_p (μm)	920	670

which was scaled. The decision to scale only a section of the combustor was based on the observations of Glicksman and McAndrews (1985) and Glicksman et al. (1987). They found that the bubble distribution is nearly uniform throughout the bed cross-section for large-particle bubbling fluidized beds containing a large array of horizontal tubes.

Figure 2 is a sketch of the MIT cold model. Air from a main blower unit enters the inlet plenum of the model and then passes through a distributor plate fluidizing the bed material. The expanded bed height corresponds approximately with the top of the tube bank. The air leaving the bed passes through a cyclone to capture elutriated bed material. Finally the air exhausts into the room after passing through a filter box.

A granular linear low-density polyethylene manufactured by Union Carbide was chosen as the cold bed material. It has a solid density of

Figure 1. Tidd boiler enclosure with scaled section designated

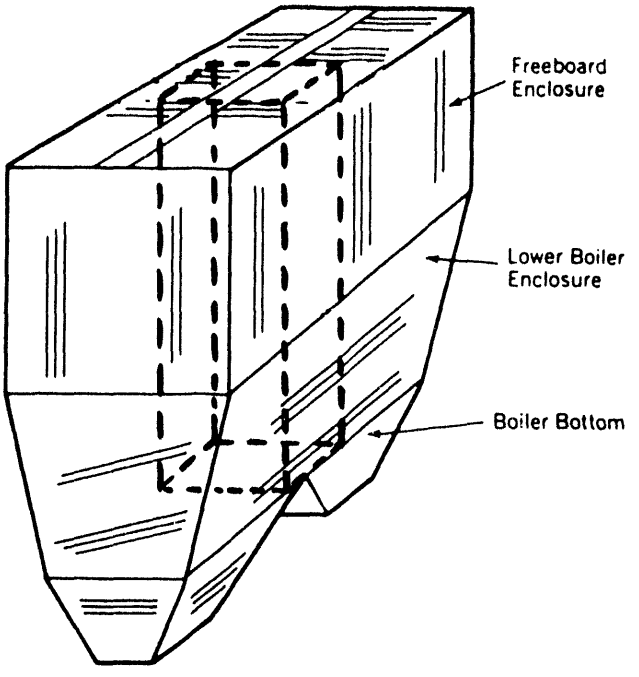

Figure 2. MIT cold model of Tidd PFBC

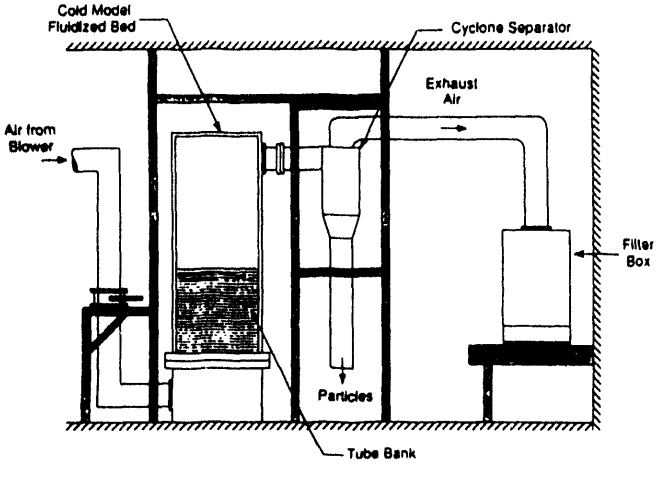

$918\ kg/m^3$ which allows the hot bed density ratio to be matched within 5%. The cold bed material particle sphericity is 0.85 which matches the hot bed value within 4%. Approximately 300 lbs of this material is required to achieve the full bed height.

Preliminary scaling comparisons

Some uncertainty exists in the mean particle diameter and particle size distribution of the Tidd bed material. It is not possible to obtain a particle sample from the center of the bed. Samples typically are taken from bed drains or sorbent reinjection vessels. These may or may not be representative of the material in the bed. The cold bed data presented here were taken with a mean particle diameter of approximately 420 μm which is smaller than the 670 μm particle diameter required to match all the scaling parameters. This was done to evaluate the sensitivity of the scaling to particle size. In the cold bed data u_o/u_{mf} and the particle size distribution were not matched between the hot and cold beds while u_o^2/gD, ρ_f/ρ_s, and L/D were matched. Table 2 summarizes the operating conditions for the hot bed and the cold model. Table 3 compares the values of the simplified scaling parameters for the two beds.

Figure 3 compares the Tidd bed and cold model solid fraction profiles. The solid fraction is the fraction of the bed between two pressure taps which is occupied by the bed material. In gas fluidized beds it is given approximately by

$$1 - \varepsilon \approx \frac{\Delta p}{\rho_s g \Delta h} \qquad (3)$$

Figure 3 shows that in the cold model, the solid fraction is lower (higher voidage) in the bottom of the bed and approximately constant in the upper part of the bed. The hot bed data appear to exhibit a similar trend. One possible explanation for the lower solid fraction in the bottom of the bed could be the presence of small slow moving bubbles causing a high voidage. As the bubbles coalesce they rise faster reducing the voidage. Throughout the tube bank the bubbles are prevented from growing any further producing a fairly flat solid fraction profile. The disagreement between the hot and cold bed solid fraction profiles in the bottom of the bed may be due to the mis-scaled particle size in the cold model. It is difficult to draw any definitive conclusions until data are taken from the cold model with all the scaling parameters matched. More hot bed data is needed to verify the preliminary data.

Table 2. Tidd PFBC and MIT cold model operating conditions

	Tidd PFBC	MIT Cold Model (1/4 Scale)
T (°K)	1116	322
p (N/m^2)	1.013×10^6	1.013×10^5
μ (kg/m-s)	4.5×10^{-5}	2.0×10^{-5}
ρ_f (kg/m^3)	3.2	1.1
ρ_s (kg/m^3)	2513	918
ϕ_s	0.82	0.85
u_{mf} (m/s)	0.27	0.06
u_o (m/s)	0.91	0.45
D (m)	3.4	0.85
d_p (μm)	920	420

Table 3. Comparison of Tidd PFBC and MIT cold model scaling parameters

	Tidd PFBC	MIT Cold Model (1/4 Scale)
ρ_s/ρ_f	795	834
u_o^2/gD	0.025	0.025
u_o/u_{mf}	3.37	7.5
ϕ_s	0.82	0.85

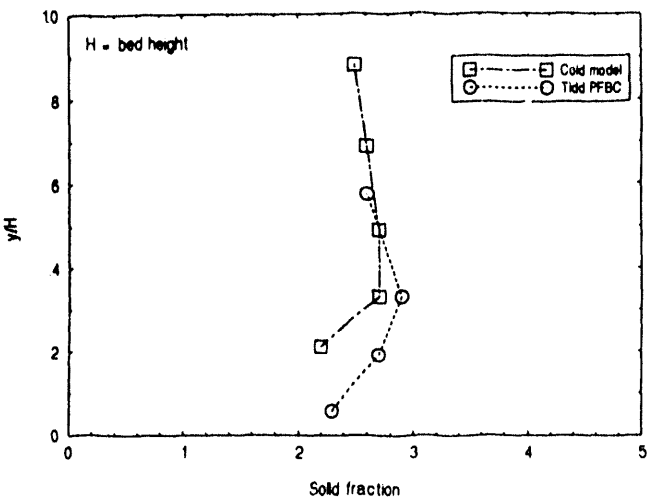

Figure 3. Comparison of Tidd and cold model solid fraction profiles

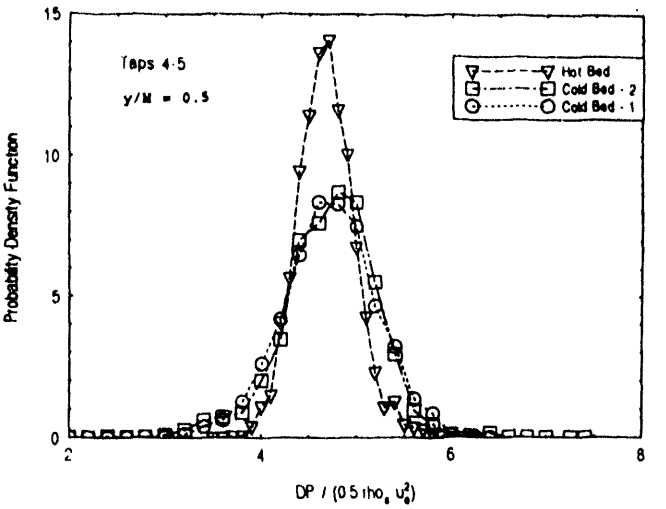

Figure 4. Comparison of probability density functions of Tidd and cold model pressure drop data

High speed time-varying pressure drop data have been taken by Babcock and Wilcox on the Tidd plant. As mentioned previously, the probability density function (PDF) and the power spectral density (PSD) are used to characterize the amplitude and the frequency of the time-varying pressure signal. The PDF measures the probability of the amplitude of the pressure fluctuations being in a certain interval. The PSD gives analogous information about the frequency of the fluctuations. Figure 4 compares the PDFs of the hot and cold bed pressure data as a function of the dimensionless pressure drop. Similarly, Figure 5 compares the PSD of the hot and cold bed pressure data as a function of the dimensionless frequency. These two figures correspond to a single differential pressure location in the bed, similar plots could be generated for the other locations in the bed. Again, due to the fact that all the scaling parameters have not been matched it is presently difficult to draw any conclusions. When data are taken on the cold model with all the scaling parameters matched, it will be possible to assess the level of agreement with the Tidd PFBC, and to evaluate the sensitivity of the scaling to the particle size.

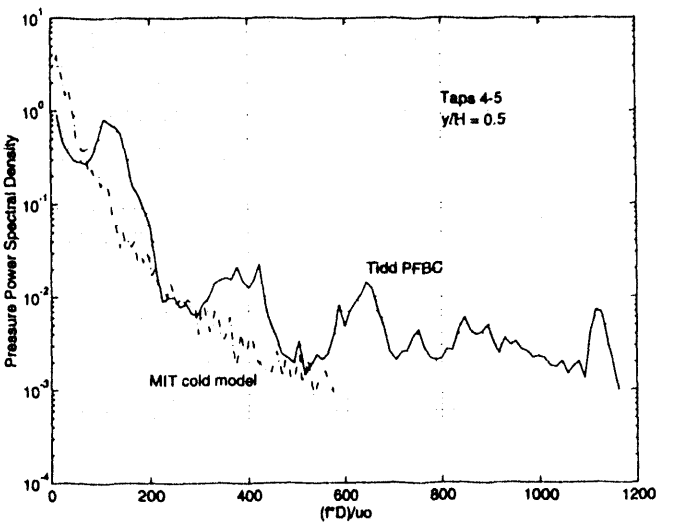

Figure 5. Comparison of power spectral densities of Tidd and cold model pressure drop data

FUTURE WORK

Hydrodynamic scaling

The properly scaled particle size and size

distribution must be attained in the cold model. This will permit direct scaling comparisons between the Tidd PFBC and the MIT cold scale model. Additional high speed hot bed data must also be obtained to corroborate the validity of the initial set of Tidd pressure data. Based on the results of the scaling comparison, the cold model tube bank details will be refined, if necessary, to obtain good agreement between the hot bed and the cold model. Current plans are to complete this work by August 1994.

Solids mixing

Once the cold scale model has been verified it will be possible to begin to investigate the solids mixing in the bed. The emphasis will be on obtaining information to help designers determine the necessary fuel feed spacing. Studies will also be done to evaluate the effects of varying bed operating and geometric parameters on solids mixing.

Tidd support

One of the advantages of having a cold scale model of an existing combustor is that it can be used as a diagnostic tool to evaluate problems related to the bed hydrodynamics. Tidd has experienced a number of problems related to solids mixing including: insufficient heat transfer surface area, poor fuel distribution, and sinter formation. It is often difficult to perform the detailed measurements necessary to solve a problem in the hostile environment of a combustor. AEP is currently interested in trying to obtain information from the cold model to give them guidance in addressing some of these problems.

NOMENCLATURE

D	Reference bed dimension
d_p	Surface-volume mean particle diameter
g	Acceleration due to gravity
L	Bed dimension
PSD	Dimensionless particle size distribution
u_{mf}	Minimum fluidization velocity
u_o	Gas superficial velocity
Δh	Distance between pressure taps
H	Expanded bed height
Δp	Incremental pressure drop
ε	Voidage
μ	Fluidizing gas dynamic viscosity
ϕ_s	Particle sphericity
ρ_f	Fluidizing gas density
ρ_s	Particle solid density

REFERENCES

Almstedt, A.E. and Zakkay, B., 1990, "An Investigation of Fluidized-Bed Scaling - Capacitance Probe Measurements in a Pressurized Fluidized-Bed Combustor and a Cold Model Bed," Chemical Engineering Science, 45, 4, pp. 1071-1078.

Anderson, T.B. and Jackson, R., 1967, "A Fluid Mechanical Description of Fluidized Beds - Equations of Motion," I&EC Fundamentals, 6, 4, pp. 527-539.

Chang, H. and Louge, M., 1992, "Fluid Dynamic Similarity of Circulating Fluidized Beds," Powder Technology, 70, pp. 259-270.

Glicksman, L.R., 1984, "Scaling Relationships for Fluidized Beds," Chemical Engineering Science, 39, 9, pp. 1373-1379.

Glicksman, L.R., 1988, "Scaling Relationships for Fluidized Beds," Chemical Engineering Science, 43, 6, pp. 1419-1421.

Glicksman, L.R., Westphalen, D., Brereton, C., and Grace, J., 1991, "Verification of Scaling Laws for Circulating Fluidized Beds," in Circulating Fluidized Bed Technology III, P. Basu, M. Horio, and M. Hasatani, eds., Pergamon Press, p. 119.

Glicksman, L.R., Hyre, M.R., and Woloshun, K., 1993, "Simplified Scaling Relationships for Fluidized Beds," Powder Technology, 77, pp. 177-199.

Glicksman, L.R., Lord, W.K., and Sakagami, M., 1987, "Bubble Properties in Large-Particle Fluidized Beds," Chemical Engineering Science, 42, 3, pp. 479-491.

Glicksman, L.R., and McAndrews, G., 1985, "Effect of Bed Width on the Hydrodynamics of Large Particle Fluidized Beds," Powder Technology, 42, pp. 159-167.

Grace, J.R., 1982, "Fluidized-Bed Hydrodynamics," Chapter 8.1, Handbook of Multiphase Systems, ed. G. Hestroni, Hemisphere, Washington, DC.

Kinsinger, F.L., 1990, "PFBC System Modularity," Babcock & Wilcox Technical Paper BR-1409, Presented to American Power Conference, Chicago, IL.

Newby, R.A. and Keairns, D.L., 1986, "Test of the Scaling Relationships for Fluid-Bed Dynamics, Fluidization V, Engineering Foundation, New York, pp. 31-38.

Nicastro, M.T. and Glicksman, L.R., 1984, "Experimental Verification of Scaling Relationships for Fluidized Bed," Chemical Engineering Science, 39, 9, pp. 1381-1391.

Roy, R. and Davidson, J.F., 1989, "Similarity Between Gas-Fluidized Beds at Elevated Temperature and Pressure," Fluidization VI, Engineering Foundation, New York, pp. 293-300.

Valenzuela, J.A. and Glicksman, L.R., 1984, "An Experimental Study of Solids Mixing in a Freely Bubbling Two-Dimensional Fluidized Bed," Powder Technology, 38, p. 63.

Westphalen, D., 1993, "Scaling and Lateral Solid Mixing in Circulating Fluidized Beds," Ph.D. Thesis, Department of Mechanical Engineering, Massachusetts Institute of Technology.

P14 Evaluation of Options for CO_2 Capture/Utilization/Disposal

CONTRACT INFORMATION

Contract Number	DE-92MC29220
Contractor	Argonne National Laboratory 9700 S. Cass Argonne, IL 60439 (708) 252-5913
Contractor Project Manager	David K. Schmalzer
Principal Investigators	Richard D. Doctor C. David Livengood
METC Project Manager	Richard A. Johnson
Period of Performance	June 1, 1993 to June 1, 1994

Schedule and Milestones

FY 94 Program Schedule

	S	O	N	D	J	F	M	A	M	J	J	A	S
IGCC/Commercial CO_2	———												
IGCC/Developmental CO_2		———											
IGCC/O_2/Commercial CO_2				———									
IGCC/O_2/Developmental CO_2								———					

OBJECTIVE

The project objective is to develop engineering evaluations of technologies for the capture, use, and disposal of carbon dioxide (CO_2). This project emphasizes CO_2-capture technologies combined with integrated gasification combined-cycle (IGCC) power systems. Complementary evaluations address CO_2 transportation, CO_2 use, and options for the long-term sequestration of unused CO_2. Commercially available CO_2-capture technology is providing a performance and economic baseline against which to compare innovative technologies. The intent is to provide the CO_2 budget, or an "equivalent CO_2" budget associated with each of the individual energy-cycle steps in addition to process design capital and operating costs. The value used for the "equivalent CO_2" budget is 1 kg CO_2/kWhe.

This study took the gasifier output from an IGCC plant through water-gas shift and then to either amine, low-pressure glycol, chilled methanol, or hot potassium carbonate CO_2

recovery prior to the combustion turbine. Carbon dioxide recovery from the main stack was set at 90%, and the combustion turbine now was fed a high hydrogen content fuel. From the IGCC plant, a 500-km pipeline took the CO_2 to geological sequestering. For these cases, the net electric power production was reduced by 73.6 - 185.1 MW with a 0.29 - 0.53 kg/kWhe CO_2 release rate (when make-up power was considered.) Life-cycle CO_2 sequestering costs ranged from 113 - 201 $/ton CO_2. Two additional life-cycle energy balances for emerging technologies were considered including: 1) high-temperature CO_2 separation with calcium- or magnesium-based sorbents, and 2) ambient-temperature polymer membranes for acid-gas removal.

BACKGROUND INFORMATION

The location of the IGCC plant is specified as the midwestern United States. We have set the location as 160 km. by rail from the Old Ben No. 26 coal mine in Seeser, IL, the source of Illinois #6 coal used in the study. Details of the IGCC portion of the system are taken from a previous report (Southern Company Services, 1990), which describes a plant utilizing an air-blown gasifier with in-bed sulfur removal. The base case is a 458-MW IGCC system using an air-blown Kellogg-Rust-Westinghouse (KRW) agglomerating fluidized bed gasifier, Illinois #6 bituminous coal feed and in-bed sulfur removal. Mining, feed preparation and conversion result in a net electric power production of 453 MW with a 0.835 kg/kWhe CO_2 release rate.

PROJECT DESCRIPTION

The gasifier output ran through water-gas shift and then to CO_2 recovery prior to the combustion turbine. Carbon dioxide recovery from the main stack was set at 90%, and the combustion turbine now was fed a high hydrogen content fuel. From the IGCC plant, a 500-km pipeline took the CO_2 to geological sequestering.

Coal and Limestone Mining

Old Ben No. 26 is an underground mine with an associated coal-preparation plant. The IGCC power plant is assumed to be 160 km from the mine, shipment of the coal being by rail using a unit train. In order to supply the 152,667 kg/h of coal required by the IGCC plant, the mine and preparation plant combination requires 2.42 MW of power and produces 2,418 kg/h of CO_2. Another 637 kg/h of CO_2 is produced by the diesel-powered rail transportation.

Limestone is used for in-bed sulfur capture in the gasifier. It is assumed that the limestone is extracted from a surface mine (quarry) about 160 km from the plant and transported by rail to the plant site. A total of 39,795 kg/h of limestone is used by the process, giving an energy consumption for extraction of 0.257 MW with an associated CO_2 production of 257 kg/h. Shipment of the limestone by diesel-powered train produces another 140 kg/h of CO_2.

Coal and Limestone Handling

The coal handling system at the plant includes equipment for unloading the coal from the unit train, passing it through preparation and crushing, and then conveying it to 14-h storage silos. The coal is crushed and dried in a series of three fluidized-bed roller mills where the heat for drying is provided by the hot (760 °C) flue gas from the IGCC sulfator process. This drying results in a significant CO_2 emission from the energy cycle that is not reclaimed, but presents a possible opportunity for further reductions. The CO_2 emissions from the sulfator are 13,099 kg/h.

Limestone is crushed in two pulverizers and then pneumatically conveyed to a 24-h storage silo and a 2-h storage bunker before being mixed with the coal in the gasifier surge bins. Energy consumption in this part of the plant is 3.58 MW.

Integrated Gasification Combined-Cycle Base Case

The base case for the comparisons uses air-blown KRW fluidized-bed gasifiers and in-bed sulfur removal. A simplified schematic for this process appears in Figure 1. The system includes two heavy-duty industrial gas turbines (1260 °C firing temperature) coupled with a reheat steam-turbine bottoming cycle. Spent limestone and ash from the gasifier are oxidized in an external sulfator prior to disposal. As noted previously, the sulfator flue gas is taken to the coal-preparation operation for drying coal and is not integrated into the later CO_2 recovery operation, nor is the small amount (158 kg/h) of CO_2 that is emitted from the gasifier lock hoppers.

The hot-gas cleanup system for particulate matter consists of a cyclone followed by a ceramic-candle-type filter. Solids collected are sent to the external sulfator prior to disposal. Gas temperatures are maintained at approximately 540 °C. Supplemental hot-gas desulfurization is accomplished in a fixed-bed zinc-ferrite system. Off-gas from the regeneration of this polishing step is recycled to the gasifier for capture.

The balance of the in-plant consumption of electricity is 33.0 MW, with a main stack CO_2 emission of 362,820 kg/h. The gross IGCC electric power output is 493.8 MW; the total in-plant consumption is subtracted to yield 457.2 MW at the busbar.

Integrated Gasification Combined-Cycle with CO_2 Recovery

Several changes were made to the base case IGCC plant in order to incorporate CO_2 recovery, as shown in Figure 2. These changes entailed processing the cleaned fuel gas through a "shift" reaction to convert the CO to CO_2, recovering the CO_2, and then combusting the low-CO_2 fuel gas in a modified turbine/steam cycle to produce electricity. Gas cleaning and sulfator performance were considered to be unaffected by these changes.

The fuel gas from the KRW process is high in CO. Conversion of the CO to CO_2 in the combustion process would result in considerable dilution of the resulting CO_2 with nitrogen from the combustion air and with water from the combustion reaction. If the CO_2 is removed prior to combustion, a substantial savings in the cost of the CO_2 recovery system is possible because of reduced vessel size and solvent flow rate. The CO in the fuel gas must first be converted to CO_2 by the shift reaction:

$$CO + H_2O \Longrightarrow CO_2 + H_2 .$$

The resulting CO_2 can then be recovered, leaving a hydrogen-rich fuel for use in the gas turbine.

The shift reaction is commonly accomplished in a catalyst-packed tubular reactor. A relatively low-cost iron-oxide catalyst is effective in the temperature range of 340 to 590 °C. Below that range, a more expensive copper-oxide catalyst is required. While the equilibrium concentrations of products are favorable at lower temperatures, this consideration must be balanced against the need for larger reactors. In view of these conflicting considerations, high CO_2 recovery is best achieved by staged reactors that allow for cooling between stages. A two-stage system was chosen for this study, configured to achieve 95% conversion of CO to CO_2.

A number of CO_2-removal technologies are commercially available for application to IGCC systems. However, all of these options involve cooling or refrigerating the gas stream, with an attendant loss of thermal efficiency. To minimize the loss, the heat removed during cooling must be recovered and integrated into the system. Several options for this integration were evaluated, including steam generation alone, fuel-gas

preheating with supplemental steam generation, and fuel-gas saturation and preheating. In the last case, which was the one chosen for this study, moisture condensed from the fuel gas prior to CO_2 recovery is injected into the clean fuel-gas stream as it is heated by recovered heat following CO_2 removal. This allows additional heat to be absorbed before combustion and increases the mass flow rate through the gas turbine. The balance of the thermal energy is used in the heat-recovery steam generator for feedwater heating and steam generation.

The commercial CO_2 recovery processes operate by absorption of the CO_2 in a liquid solvent and subsequent regeneration of the solvent to release the CO_2. The temperature of absorption is solvent-specific. In general, however, the solvents have low boiling points so that substantial cooling of the synthesis gas is required, as noted above. Furthermore, lower temperatures favor absorption, thereby reducing the necessary solvent flow rate. This implies a need for further cooling or refrigeration of the solvent, with additional energy losses. The regeneration of the solvent is also energy-intensive for most processes, since it is usually accomplished by flashing (pressure reduction) and/or heating. If flashing is employed, repressurization of the solvent is required. Heating is generally accomplished by the extraction of steam from the steam cycle.

Five alternative CO_2-recovery processes have been evaluated to date: (1) high-pressure (1000-psi) absorption by a glycol-type solvent with regeneration by flashing, (2) low-pressure (250-psi) absorption by a glycol-type solvent with regeneration by flashing, (3) absorption by monoethanolamine (MEA) with regeneration by throttling and heating via a reboiler, (4) absorption by hot potassium carbonate with regeneration by throttling and heating, primarily by a reboiler, and (5) absorption by low-temperature methanol with regeneration by thermal stripping and distillation.

From an energy perspective, the glycol options have the advantage. This is particularly true for the low-pressure system, which does not require compression of the synthesis gas prior to absorption. The low-pressure glycol system was the most favorable of any of the systems surveyed. The busbar rating of the plant dropped to 473 MW, from which 87.4 MW of internal plant use must be subtracted. Total CO_2 emissions from the preparation plant through compression to 2100 p.s.i. pipeline pressure were 47,267 kg/h.

Pipeline Transport of CO_2

Once the CO_2 has been recovered from the fuel-gas stream, its transportation, utilization, and/or disposal remain as significant issues. Carbon dioxide represents a large-volume, relatively low-value by-product that cannot be sequestered in the same way as most coal-utilization wastes (i.e., by landfilling). Large volumes of recovered CO_2 are likely to be moved by pipeline. In some cases, existing pipelines could be used, perhaps in a shared mode with other products. In other cases, new pipeline construction would be required. Costs for pipeline construction and use vary greatly on a regional basis within the United States.

The recovered CO_2 (328,810 kg/h) represents about four million normal cubic meters per day (4×10^6 Nm^3/d) of gas volume. A supercritical CO_2 pipeline was designed for the transport of this recovered gas. The booster compression for this system contributed an additional 2,066 kg/h of CO_2 emissions and 2.07 MW of power use.

CO_2 Sequestering

It has been proposed that CO_2 be disposed of in the ocean depths. However, many engineering and ecological concerns associated with such an option remain unanswered, and the earliest likely reservoir is a land-based geological

repository. A portion of the CO_2 can be utilized for enhanced oil recovery (EOR), which sequesters a portion of the CO_2, or it can be completely sequestered in depleted gas/oil reservoirs and nonpotable aquifers. Both the availability of these zones and the technical and economic limits to their use need to be better characterized. The energy required at the sequestering site was analyzed, recognizing that the power required for compression will rise throughout the life-cycle of these sequestering reservoirs. However, it was found that the first reservoirs that would be used will in fact be capable of accepting all IGCC CO_2 gas for a 30-yr period without requiring any additional compression costs for operation.

RESULTS

Energy Balance

Comparisons of the system CO_2 and energy balances are given in Fig. 3. The amounts of raw materials (coal and limestone) supplied to the plant are assumed to be constant for both the base and CO_2-recovery cases. However, gross power generation varies with changes in internal energy use (primarily affecting the steam turbine output). Energy use for plant auxiliaries and the CO_2 recovery process is subtracted from the gross generation to yield the net busbar output. This must be further reduced by the external power consumption to yield the net system energy output.

For the CO_2 recovery cases, the system efficiency is reduced from the base-case value of 39.6% to 34.5% with a reduction of about 74 MW in the net system output. If the energy used for compression of the CO_2 at the IGCC plant is combined with the booster-station requirements, nearly one-half of that reduction is seen to be due to transportation of the CO_2 to the disposal site. Nevertheless, the total CO_2 emissions are reduced to only 16% of those in the base case, and the emission rate is reduced from 0.835 kg/kWh to only 0.156 kg/kWh. It should be noted that replacement of the "lost" 74 MW would likely entail additional CO_2 emissions that are not accounted for here.

Economics

The incremental capital and operating costs associated with CO_2 recovery appear in Table 1. While the equipment installed in the base plant has not changed, the cost in terms of $/kW escalates because of the derating of the plant. The annual costs of operating the plant in terms of $/yr uses a 4th quarter 1993 base, and assumes that the shift, CO_2 recovery and booster sections of the plant will not impact overall plant availability.

The base case power cost of 49.5 mills/kWh is increased by nearly 74% in the most favorable case to 86.1 mills/kWh. Part of this cost is charged to the purchase of 74 MW of make-up power for this case at a cost of 60 mills/kWh.

FUTURE WORK

The project will continue to evaluate cases for advanced technologies in oxygen-blown IGCC systems during the remaineder of the fiscal year. The results presented in this study show the value of approaching the issue of IGCC power generation with CO_2 recovery from a full life-cycle analysis.

ACKNOWLEDGMENT

The authors gratefully acknowledge the support and guidance provided by Dr. Richard A. Johnson of the Morgantown Energy Technology Center, who is the project officer for this research.

REFERENCES

1. Southern Company Services, Inc., et al., 1990, *Assessment of Coal Gasification/Hot Gas Cleanup Based Advanced Gas Turbine Systems*, DOE/MC/26019.3004 (DE91002084), prepared by Southern Company Services, Inc., Birmingham, Ala., for the U.S. Department of Energy, Morgantown Energy Technology Center, Morgantown, W.Va.

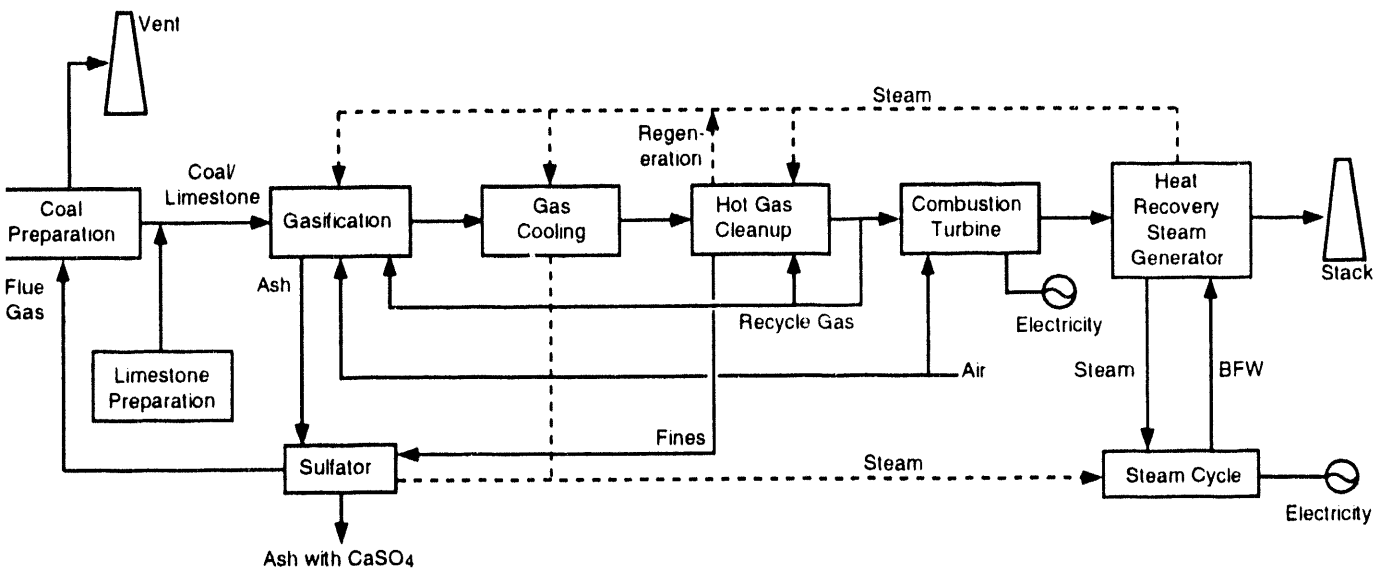

Figure 1. Block diagram of the base case IGCC system.

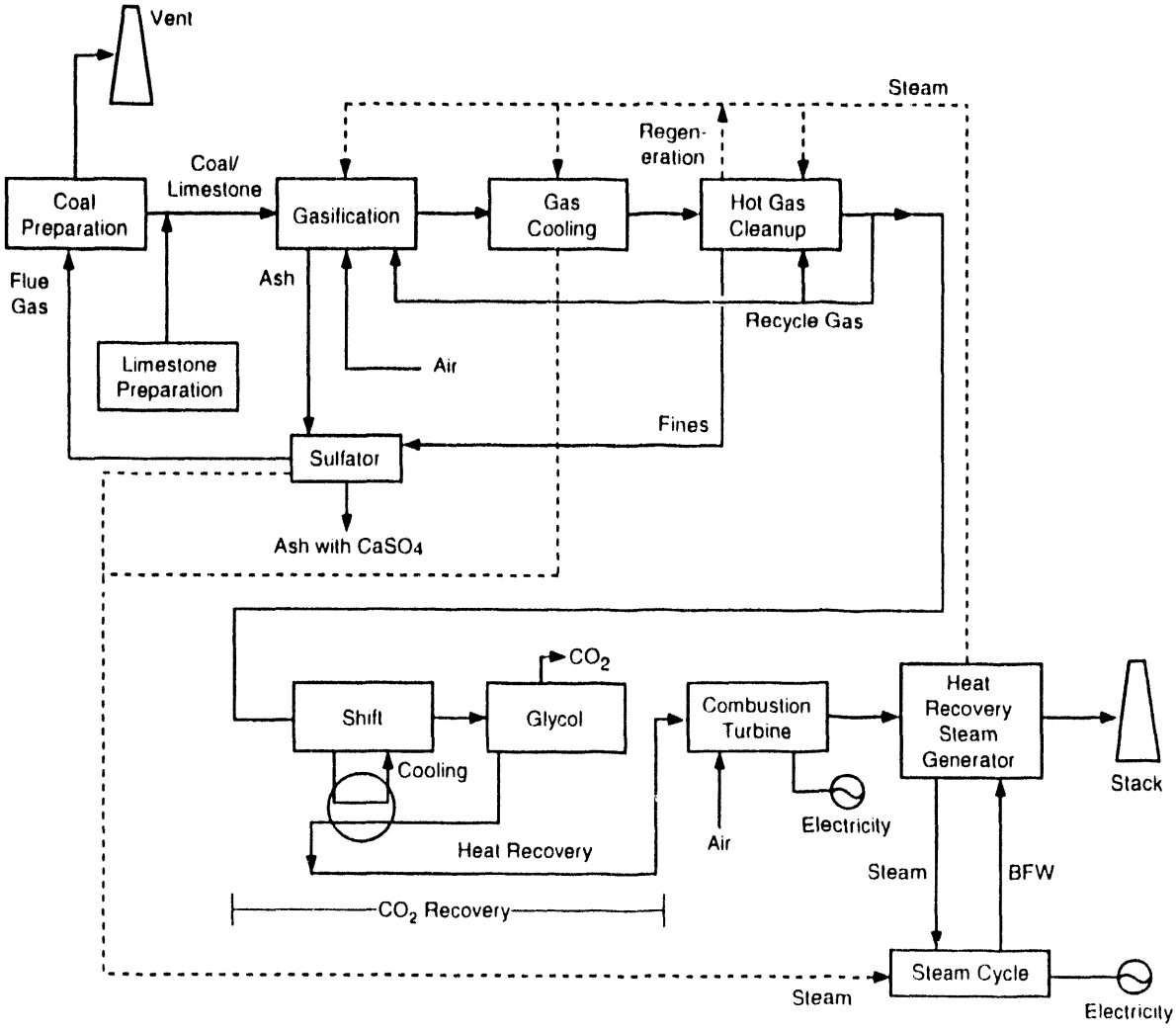

Figure 2. Block diagram of the IGCC system with CO_2 recovery

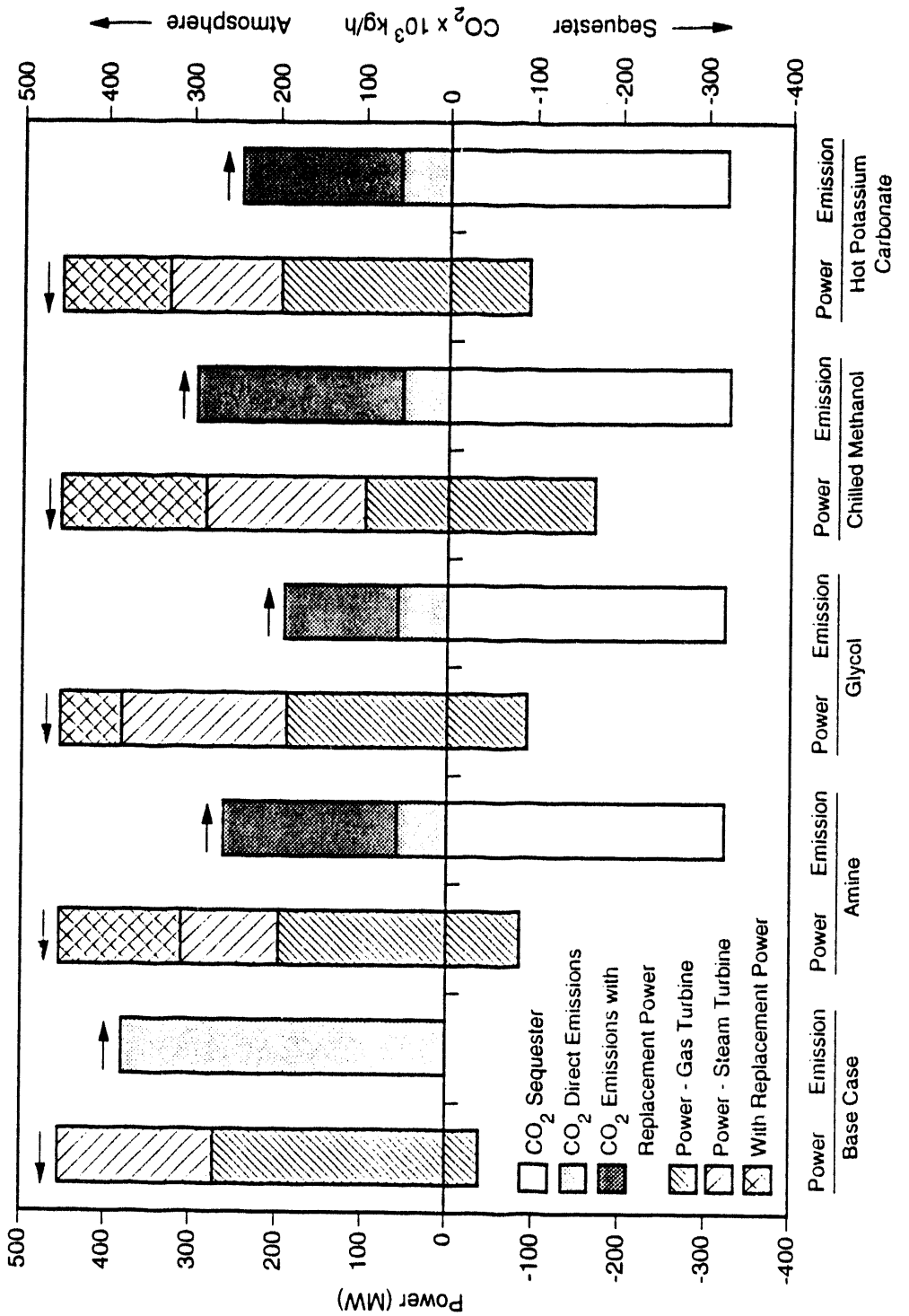

Figure 3. Net Power Generation and Associated Carbon Dioxide Inventory

Table 1. Comparitive Costs of IGCC with Shift/CO_2 Recovery/Pipeline

Component	Unit	KRW Base	MEA	Glycol	Methanol	K-Carbonate
Base Plant Capital	$/kW	1342	1945	1591	2238	1842
CO_2 Control Capital	$/kW	0	647	529	861	615
Power Plant Annual Cost	$/yr	$128,157,363	$148,835,848	$148,325,526	$160,519,522	$148,441,638
Base Plant Power Cost	mills/kWh	49.5	57.5	57.3	62.0	57.4
Pipeline (500 km)	mills/kWh	0.0	19.1	19.1	19.1	19.1
Replacement Power	mills/kWh	0.0	19.0	9.7	24.4	16.7
Net Power Cost*	**mills/kWh**	**49.5**	**95.6**	**86.1**	**105.6**	**93.1**
Coal Energy Input	10^6Btu/h	3940	3940	3940	3940	3940
Busbar Power Output	MW	493.80	395.50	473.00	439.10	420.30
In Plant Power Use	MW	36.63	80.13	87.35	164.98	87.19
Net Plant Output	**MW**	**457.17**	**315.37**	**385.65**	**274.12**	**333.11**
Net Heat Rate	Btu/kWh	8618	12493	10217	14373	11828
Thermal Efficiency - HHV	%	39.62	27.33	33.42	23.76	28.87
Out of Plant Power Use	MW	2.80	4.87	4.87	4.90	4.87
Net Energy Cycle Power	**MW**	**454.37**	**310.50**	**380.78**	**269.22**	**328.24**
Net Energy Cycle Heat Rate	Btu/kWh	8671	12689	10347	14635	12003
Thermal Efficiency - HHV	%	39.38	26.91	33.00	23.33	28.45
Net Energy Cycle Power	MW	454.37	310.50	380.78	269.22	328.24
Replacement Power	MW	0.00	143.87	73.59	185.15	126.13
Net Grid Power	**MW**	**454.37**	**454.37**	**454.37**	**454.37**	**454.37**

*All power costs on the basis of Net Grid Power

P15

Absorption of Hydrogen Sulfide by Zinc Ferrite in the Temperature Range 315 to 538°C (600 to 1,000°F)

Thomas Grindley
Morgantown Energy Technology Center

C. Elaine Everitt
EG&G Technical Services of West Virginia

BACKGROUND AND OBJECTIVE

The high-temperature, regenerable, desulfurization sorbents under development at METC for use in advanced power systems incorporating coal gasification have been designed to operate at temperatures upwards of about 538°C (1,000°F). This temperature has been thought to be optimal, taking into account such factors as higher sorbent reactivity, increased thermodynamic efficiency, and regeneration temperature.

Recent revision of total system considerations indicates that, in certain circumstances, it may be desirable to operate these sorbents at lower temperatures because of materials considerations. Therefore, a small laboratory investigation of the desulfurization performance of zinc ferrite, one of the sorbents under development, was conducted in the temperature range 315 to 538°C (600 to 1,000°). A previous study (Grindley 1982) had indicated a dramatic decline of zinc ferrite's desulfurization performance at 427°C (800°F) compared to that at 538°C (1,000°F).

A number of sulfidation tests were performed using a low-pressure, fixed-bed reactor and simulated gas containing hydrogen sulfide. Hydrogen sulfide breakthrough times were determined and sorbent properties, including sorbent sulfur loading, mineral properties, and porosity, were measured. An attempt was made to apply a fixed-bed simulation model to the data. These points are summarized:

Background

- Performance of regenerable hot-gas desulfurization sorbents below 538°C relatively neglected.
- Decline in rate of desulfurization known but not sufficiently quantified.

Objective

- Conduct sulfidation tests in a small fixed-bed reactor at 315 to 538°C.
- Determine hydrogen sulfide breakthrough times.
- Measure sorbent porosity by mercury porosimetry and nitrogen adsorption.
- Determine effect of sorbent reduction (i.e., $ZnFe_2O_4 \rightarrow ZnO + Fe_3O_4$) on reactivity.
- Estimate effect of sorbent pore size and crystallite size on reactivity.

PROJECT DESCRIPTION

Hot Gas Desulfurization Sorbents

The zinc ferrite sorbent studied was manufactured by United Catalysts, Inc., and designated L-2465. A zinc titanate sorbent, L-3024, also included in the study for comparison, was made by the same company. Details of the sorbents are given in Table 1.

Table 1. Fresh Sorbent Characteristics

	United Catalysts, Inc. L-2465 Zinc Ferrite	United Catalysts, Inc. L-3024 Zinc Titanate
Form	5 mm Extrudates	5 mm Extrudates
Composition	ZnO/Fe_2O_3	2 ZnO/TiO_2
Bentonite Binder (wt%)	2	3
Calcination Conditions (Hr @ °C)	2 @ 815°	2 @ 871°
Bulk Density (g/cm^3)	1.57	1.26
Crush Strength (N/mm)	24.0	35.8
B.E.T. Surface Area (m^2/g)	3.2	3.1
Median Pore Diameter, Volume (nm)	292.0	437.5
Mercury Porosity for Pores >12 nm (%)	54.5+	63.6#
Nitrogen Porosity for Pores <60 nm (%)	2.6*	2.3*
Helium Skeletal Density (g/cm^3)	5.3 g/cm^3*	5.2 g/cm^3*

+ Mercury porosity calculated using total pore volume reported by United Catalysts, Inc., and METC helium density.

Mercury porosity calculated using total pore volume reported by Coors Analytical Laboratory and METC helium density.

* Analysis performed at METC. All other data provided by United Catalyst, Inc.

Laboratory Test Unit

The test unit is the same as that used in previous studies (Grindley 1990, 1991). The process flow diagram is shown in Figure 1. The sorbent was placed in a 150-cm (60-in) long, 5-cm (2-in) diameter fused-silica reactor located within a 3-zone, clamshell, electric furnace. The reactor is shown in greater detail in Figure 2. The sorbent, in the form of extrudates, was supported by a perforated, fused-silica disc. Temperatures along the centerline of the reactor were measured by thermocouples, located inside a metal thermowell.

Gases and water are supplied through rotameters. The manifolded mixture was preheated before entering the reactor. Hot gases from the reactor were cooled by teflon condensers. The system was maintained at a positive pressure of 172 kPag (25 psig). In the sulfidation mode, gases were passed upwards through the reactor. Process conditions were recorded

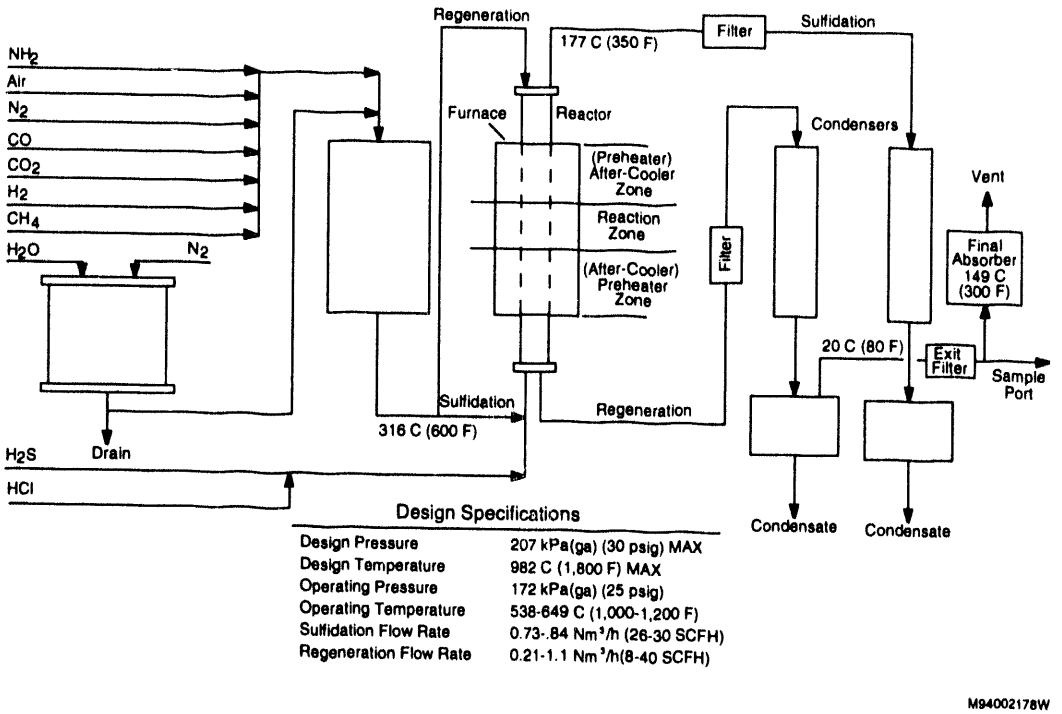

Figure 1. Hot Gas Desulfurization Lab-Scale Unit Process Flow Diagram Fixed Bed Operation

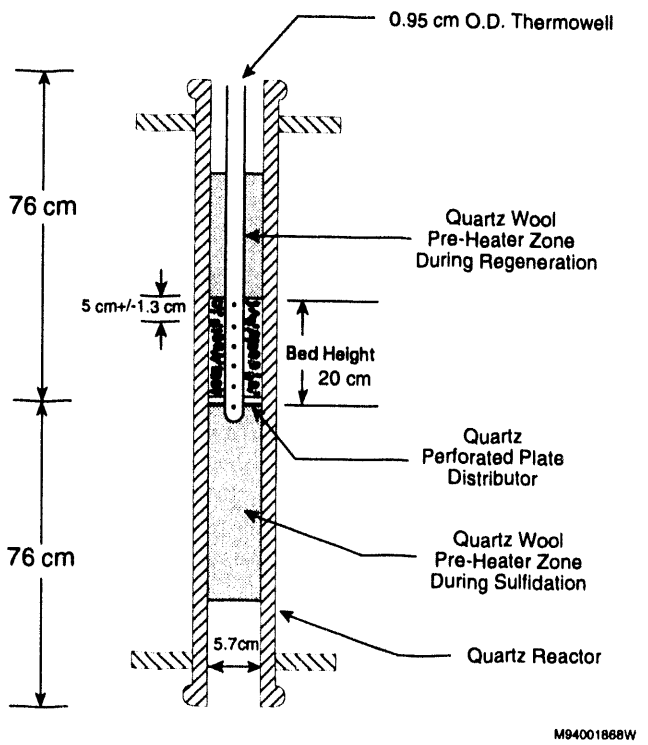

Figure 2. Reactor Details

by an automatic data acquisition and control system.

Test Unit Operation

Five sulfidation tests, 72A, 73, 74, 75, and 76, were performed on zinc ferrite and one test, 68, on zinc titanate. The tests were continued until a breakthrough point of 100 ppmv of hydrogen sulfide was reached. Nominal test conditions are detailed in Table 2. The sulfidation gas composition was typical of that from an air-blown, fluidized-bed gasifier, except for hydrogen sulfide, which was considerably higher, in order to produce an accelerated effect.

In Tests 74, 75, and 76, the sorbent was first reduced for 4 hours at 538°C (1,000°F) in the absence of hydrogen sulfide, followed by sulfidation at the prescribed test temperatures. The reduction converted the zinc ferrite into zinc oxide and magnetite ($ZnFe_2O_4 \rightarrow ZnO + Fe_3O_4$). At the end of each test, the sorbent was removed from the reactor, by vacuuming, in four sections for analysis.

EXPERIMENTAL RESULTS

Hydrogen Sulfide Breakthrough

Hydrogen sulfide breakthrough plots are shown in Figures 3 and 4. The hydrogen sulfide concentrations were measured by Gastec detector tubes, accurate to about 25 percent. Figure 3 illustrates the large effect of prereduction of zinc ferrite on the breakthrough plot at 427°C (800°F). Because sorbent reduction is rapid at 538°C (1,000°F), the breakthrough plot for Test 72A is the same as if the sorbent had been prereduced, and reduction accompanies sulfidation in this case. The plot for Test 73 at 427°C (800°F) shows a dramatic decline in breakthrough time to 1 hour from 7.5 hours in Test 72A. In Test 74, however, also at 427°C (800°F), but in which the sorbent has been prereduced at 538°C (1,000°F), the breakthrough time is somewhat greater than 5 hours, which represents a much more modest decline. The breakthrough time for zinc titanate in Test 68 at 538°C (1,000°F) is about 1.5 hours.

Figure 4 compares breakthrough times for prereduced zinc ferrite at 427°C (800°F), 371°C (700°F), and 315°C (600°F), which are contrasted with the breakthrough time for unreduced zinc ferrite at 427°C (800°F).

The decline of breakthrough time with temperature is faster than if linear. Whereas the decline for Test 72A to Test 74 (Figure 3) is from 7.5 to 5 hours, further decreases in temperature of 56°C (100°F) result in a breakthrough time of 1 hour in Test 76 and less than 0.5 hour in Test 75. The breakthrough plots are corroborated by the sorbent sulfur loadings given in Table 3. These were measured by LECO analyzer for samples at four levels in the sorbent bed. The sorbents from the various tests were analyzed by X-ray diffraction using a RIGAKU diffractometer at West Virginia University. The total integrated intensities, which are proportional to the concentrations of crystalline phases, are given in Table 4 for the predominant mineral constituents, franklinite, sphalerite, and zincite.

Of special interest is the small amount of zincite in the sorbent from Test 73, which was the only sorbent not to undergo prereduction at 538°C (1,000°F). This same phenomenon was observed in a previous investigation (Grindley 1988) in which reductive regeneration to eliminate residual sulfate was studied.

Crystallite sizes for the three mineral species were also obtained from the X-ray diffraction analyses. These are given in Table 5 where available, averaged over the sorbent bed. The crystallite size for franklinite in Test 73 is

Table 2. Nominal Test Conditions

Temperature, °C	315 - 538
Pressure, kPa(g)	172.3
Sulfidation Gas Composition, Volume %	
Nitrogen	45.6
Carbon Dioxide	5.1
Carbon Monoxide	18.3
Hydrogen	11.9
Hydrogen Sulfide	1.0
Steam	18.1
Space Velocity, hr^{-1}	2000
Bed Height, cm	20.3
Reduction Conditions when Applicable	4 Hours @ 538°C

Gas composition during reduction was sulfidation gas composition without hydrogen sulfide.

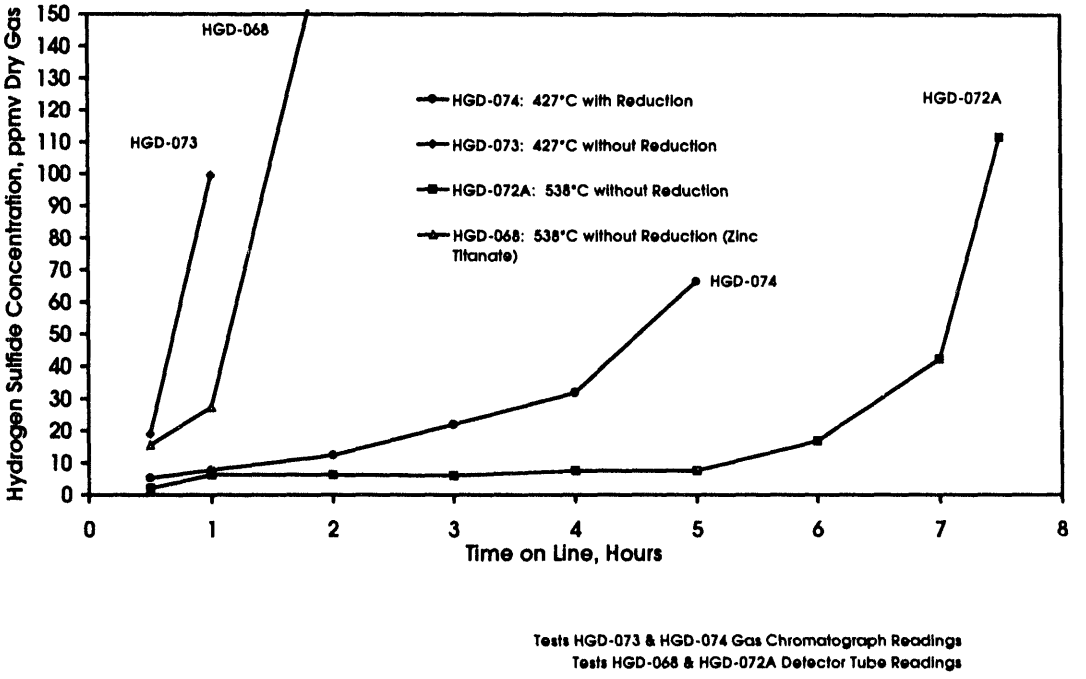

Figure 3. Hydrogen Sulfide Concentration in Exit Gas Stream Zinc Ferrite and Zinc Titanate

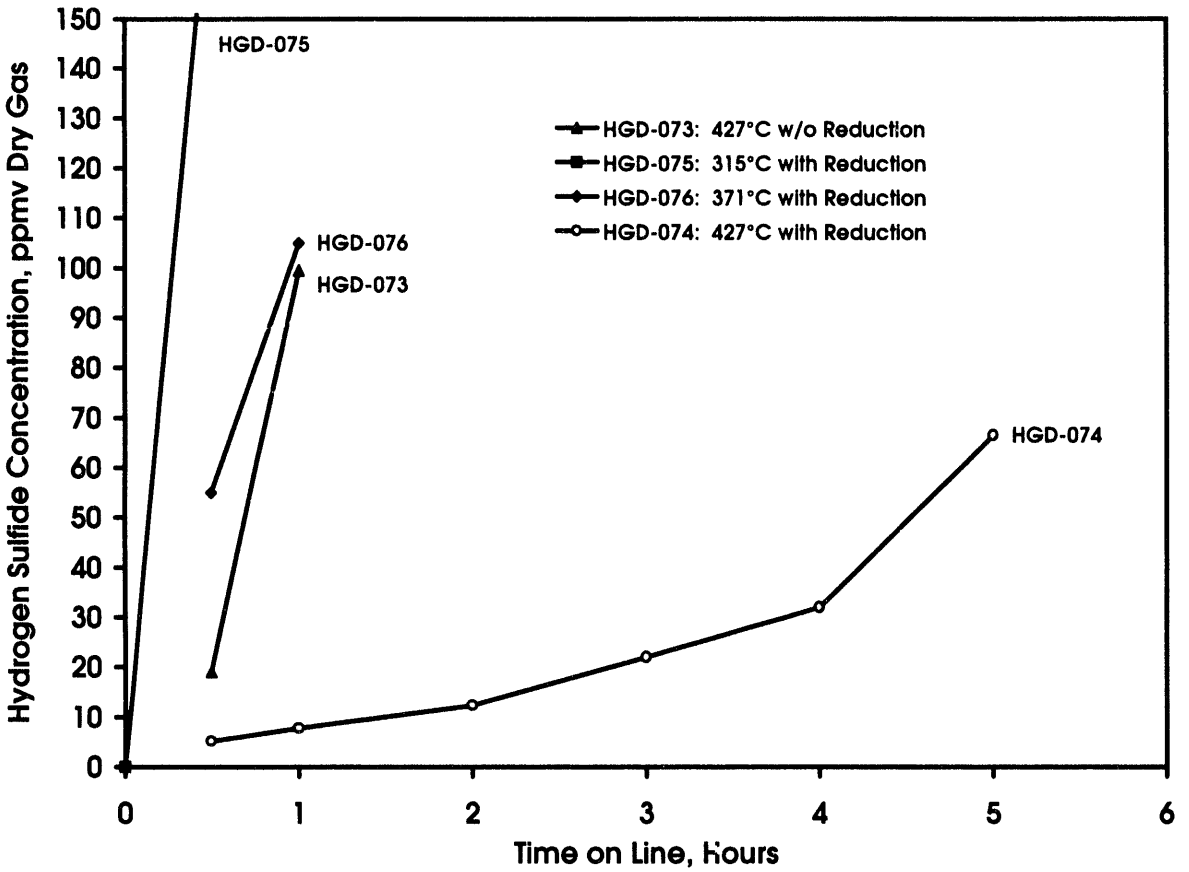

Figure 4. Hydrogen Sulfide Concentration in Exit Gas Stream: Zinc Ferrite

Table 3. Sorbent Sulfur Loading

Weight %
After Sulfidation

	Without Reduction			With Reduction		
TEST NUMBER	HGD-068			HGD-074		
Test Temperature	538°C	HGD-072A	HGD-073	427°C	HGD-075	HGD-076
Time on Stream	4 Hours	538°C	427°C	5 Hours	315°C	371°C
Sorbent	Zinc Titanate	7.5 Hours	1 Hour	Zinc Ferrite	0.5 Hour	1 Hour
Top	3.41	2.17	0.16	0.96	0.28	0.32
Top Middle	12.40	9.83	0.46	4.77	0.70	0.76
Bottom Middle	14.70	19.90	1.18	9.66	0.98	2.01
Bottom	19.20	28.50	3.80	18.30	1.37	4.55

Analysis by ASTM D4239-83 on LECO SC32 instrument.

Table 4. X-Ray Diffraction Analysis, % Total Integrated Intensity

United Catalysts, Inc., L-2465 Zinc Ferrite
After Sulfidation

	Without Reduction		With Reduction		
TEST NUMBER Test Temperature	HGD-072A 538°C	HGD-073 427°C	HGD-074 427°C	HGD-075 315°C	HGD-076 371°C
		TOP OF BED			
Franklinite $ZnFe_2O_4 + Fe_3O_4$	76.8	96.2	77.0	83.8	74.4
Sphalerite, βZnS + FeS	3.0	0.6	1.8	0.0	0.0
Zincite, ZnO	15.1	0.8	16.9	16.2	25.6
		BOTTOM OF BED			
Franklinite	34.9	92.7	63.0	85.3	82.4
Sphalerite	40.3	2.9	21.9	0.0	8.9
Zincite	5.0	1.2	4.0	14.7	8.7

% Total integrated intensity is proportional to the concentration of the crystalline phase.

much larger than that for Test 74, where prereduction occurred. This is probably a factor in explaining the lower sorbent reactivity in Test 73.

Sorbent Porosity

The sorbent porosity was measured using a Micromeritics Mercury Porosimeter and a Micromeritics Digisorb BET Surface Area Analyzer. The former is applicable to pore diameters greater than about 12 nm, whereas the latter applies to pore diameters less than about 60 nm, where it is considered to be more accurate. The porosity values for large pores together with average pore diameters are given in Table 6. Those for small pores are given in Table 7.

For the top of the sorbent bed in Table 6, there appears to be a slightly greater porosity in Tests 74, 75, and 76 where prereduction occurred, than in Test 73 where it did not. Also noticeable is a marked decrease in porosity and average pore diameter with sulfidation, which is greater at the bottom of the bed. Similar results can be seen in Table 7 for small pores. Selected sorbent porosities are plotted in Figures 5, 6, and 7.

Figure 5 illustrates the large impact of sulfidation on porosity in Test 72A. The bottom of the bed is much more heavily sulfided than the top. In Figure 6, porosities at the top of the bed for Tests 72A and 73 are compared. There is an outstandingly lower porosity for small pores in the case of Test 73 where sorbent prereduction

Table 5. X-Ray Diffraction Analysis

United Catalysts, Inc., L-2465 Zinc Ferrite After Sulfidation

	Without Reduction		With Reduction		
TEST NUMBER	HGD-072A	HGD-073	HGD-074	HGD-075	HGD-076
Test Temperature	538°C	427°C	427°C	315°C	371°C
	CRYSTALLINE SIZE, nm				
Franklinite $ZnFe_2O_4 + Fe_3O_4$	73.2	136.7	87.5	NA	NA
Sphalerite, βZnS + FeS	30.1	ND	14.8	NA	NA
Zincite, ZnO	28.5	ND	35.2	NA	NA
	TOTAL INTEGRATED INTENSITY, %				
Franklinite	59.9	94.9	73.4	80.0	79.7
Sphalerite	14.8	1.3	9.6	ND	3.4
Zincite	10.2	0.9	9.9	20.0	14.0

ND = None Detected. NA = Not Analyzed. Fresh zinc ferrite sorbent crystallite size as reported by United Catalysts: > 200 nm. All values are average for the entire bed. Total integrated intensity is proportional to the concentration of the crystalline phase.

did not occur. Figure 7 shows the smaller porosity of both large and small pores for Test 73 compared to Test 74, both at the same temperature but with sorbent prereduction only for Test 74.

Dynamic Simulation Model

The fixed-bed reactor model used to fit the experimental data was similar to that developed by Louisiana State University, assuming a shrinking unreacted core regime (Focht 1986; Wang 1988). In this case, the principal reaction resistances are diffusion within the sorbent pellets and mass transfer at the pellet exteriors. The rate of the intrinsic reaction between H_2S and the interior solid surfaces is assumed to be very rapid. These conditions appear to hold for Test 72A, as evidenced by the electron microscope, x-ray sulfur map for a pellet which is about three-quarters reacted (Figure 8). The sulfur map for Test 74 at a lower temperature (Figure 9) indicates a less sharp unreacted core. The x-ray maps were obtained by a JEOL-840A Scanning Electron Microscope interfaced to a Noran Instruments 8502 Switcher System equipped with a Noran Instruments Micro-Z Energy Dispersive Spectrometer. An attempt was made to fit the experimental hydrogen sulfide breakthrough plot by employing a $T^{1.8}$ temperature dependence of the effective diffusivity in the sorbent pores and an exp (-E/RT) dependence of

Table 6. Mercury Intrusion

United Catalysts, Inc., L-2465
Zinc Ferrite
After Sulfidation

	Without Reduction		With Reduction		
TEST NUMBER	HGD-072A	HGD-073	HGD-074	HGD-075	HGD-076
Test Temperature	538°C	427°C	427°C	315°C	371°C
	LARGE PORE POROSITY, %				
Top	52.5	52.6	54.3	54.8	52.9
Top Middle	52.5	53.5	49.9	54.5	53.2
Bottom Middle	38.4	52.2	46.3	53.5	49.4
Bottom	33.6	50.3	39.4	53.1	53.6
	MEDIAN PORE DIAMETER (Volume), nm				
Top	312.6	295.5	310.8	312.0	283.8
Top Middle	308.8	298.9	282.3	288.2	290.0
Bottom Middle	265.5	274.5	267.0	283.4	264.4
Bottom	255.0	261.0	244.1	268.7	272.7

Porosity for pores < 20 nm. Analyses performed at METC except for HGD-076 performed by Micrometrics. Fresh sorbent porosity 54.5%; median pore diameter 292 nm.

the intrinsic reaction rate constant. It was hoped that the latter would account for the departure from the unreacted core regime. As can be seen, the fit is fairly good (Figure 10). The principal parameters employed in the model are listed in Table 8, and comparison is made with a previous simulation done by Harrison for a similar test (Wang 1988).

CONCLUSIONS

Below about 538°C (1,000°F), there is a rapid fall in the rate of reduction of zinc ferrite (i.e., $ZnFe_2O_4 \rightarrow Fe_3O_4 + ZnO$) in coal-derived gas. This has a large effect on the rate of sulfidation, which also falls rapidly. Therefore, for operation at temperatures lower than 538°C (1,000°F), zinc ferrite should first be prereduced. This is easily accomplished at 538°C (1,000°F) by immersion for a short time in a flow of clean coal-derived gas. Such treatment would also eliminate any residual sulfate in the sorbent from a previous oxidative regeneration. These major findings are summarized below:

- Reduction of zinc ferrite (i.e., $ZnFe_2O_4 \rightarrow Fe_3O_4 + ZnO$) is necessary for good desulfurization.
- Reduction caused formation of zinc oxide and magnetite of smaller crystallite size than original zinc ferrite.
- Reduction of zinc ferrite caused a significant increase in small pore porosity.

Table 7. Nitrogen Adsorption Percent

United Catalysts, Inc., L-2465
Zinc Ferrite
After Sulfidation

	Without Reduction		With Reduction		
TEST NUMBER	HGD-072A	HGD-073	HGD-074	HGD-075	HGD-076
Test Temperature	538°C	427°C	427°C	315°C	371°C
Top	3.15	2.60	3.02	3.01	3.18
Top Middle	2.59	2.80	3.31	3.36	2.97
Bottom Middle	2.06	3.01	2.51	3.29	3.13
Bottom	1.98	2.94	2.21	3.31	2.91

Porosity for pores < 60 nm. Analyses performed at METC. Fresh sorbent porosity 2.6%.

- Zinc ferrite can be used below 538°C (1,000°F) if an initial reduction is carried out.

ACKNOWLEDGEMENT

We acknowledge with thanks the contributions of J. A. Poston, who provided the x-ray sorbent cross-sectional sulfur maps, and E. J. Boyle, who modeled the breakthrough plots.

Table 8. Model Parameters

HGD-072A:	
Bed Length (cm)	17.8
Bed Radius (cm)	2.85
Bed Mass (g)	629
Particle Diameter (cm)	0.476
Skeletal Particle Density (g/cc)	5.3
Bulk Density (g/cc)	1.39
Gas Velocity (cm/s)	12.8
Inlet Pressure (psig)	24
Temperature (K)	818
All Runs:	
De, effective diffusivity (cm^2/hr)	90 (Harrison: 400)
k, intrinsic reaction rate ($cm^2/mol\text{-}hr$)	3×10^7 (Harrison: 3×10^7)
ka, mass transfer (cm/hr)	55800 (Harrison: 22400)
E intrinsic/R (K)	17900
De temp dependence	$(T/884.26)^{1.78}$

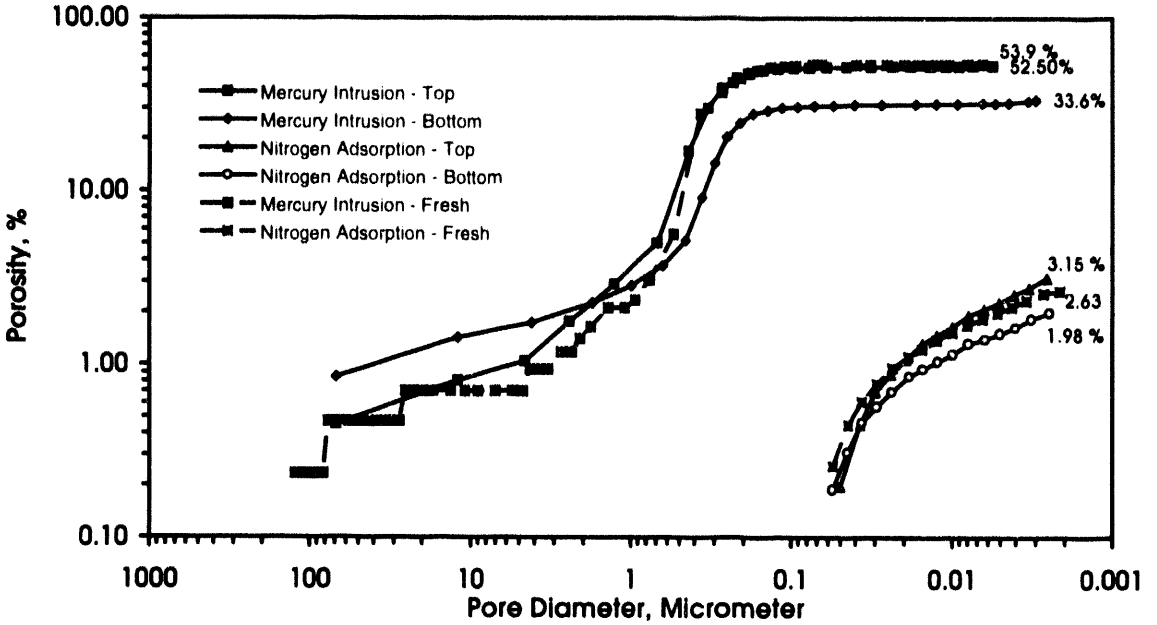

Figure 5. POROSITY vs. PORE DIAMETER
Sulfided L-2465 Zinc Ferrite Sorbent
Test No. HGD-072a 538°C

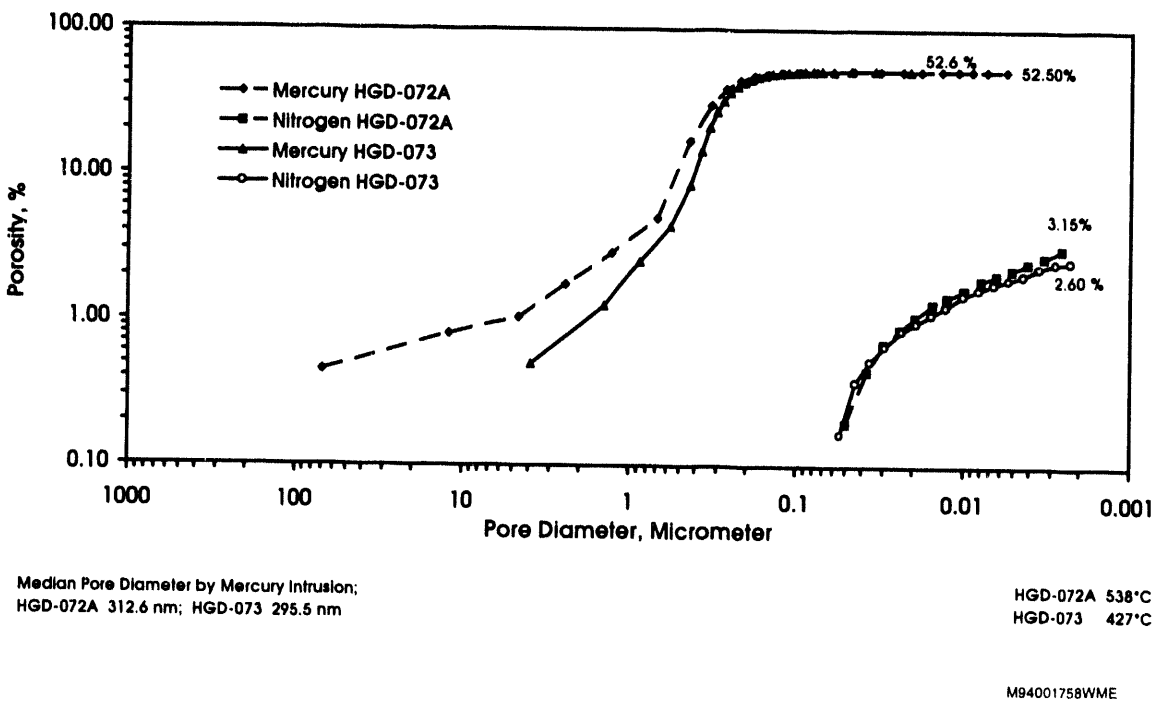

Figure 6. POROSITY vs. PORE DIAMETER
Sulfided L-2465 Zinc Ferrite Sorbent
Top of Bed

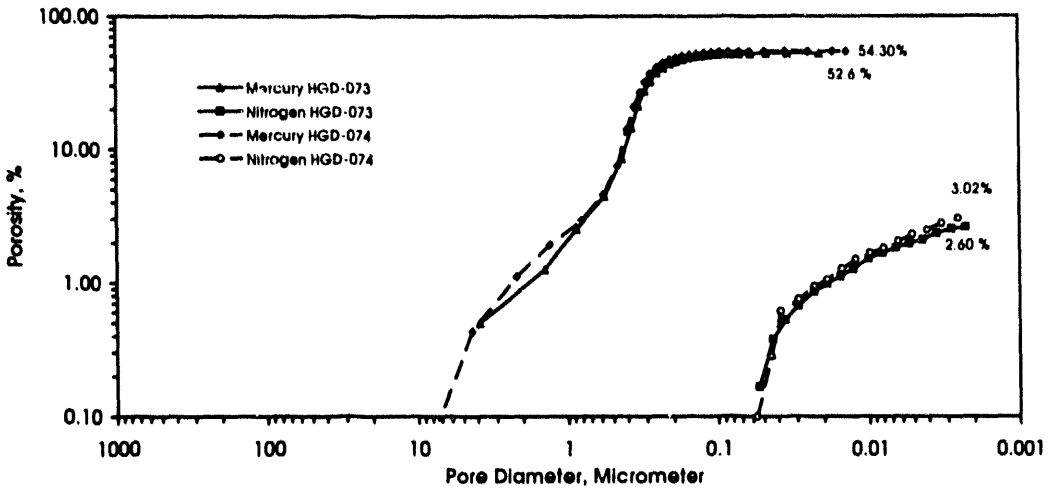

Median Pore Diameter by Mercury Intrusion;
HGD-073 295.5 nm; HGD-074 310.8 nm

HGD-073 Without Reduction
HGD-074 With Reduction

Figure 7. POROSITY vs. PORE DIAMETER
Sulfided L-2465 Zinc Ferrite Sorbent
Top of Bed

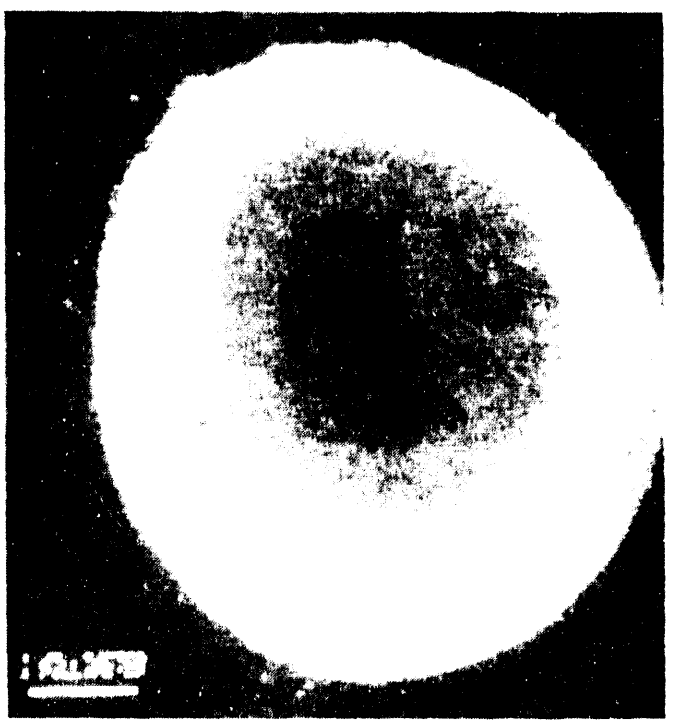

Figure 8. Zinc Ferrite Test 72A
Sulfur Map

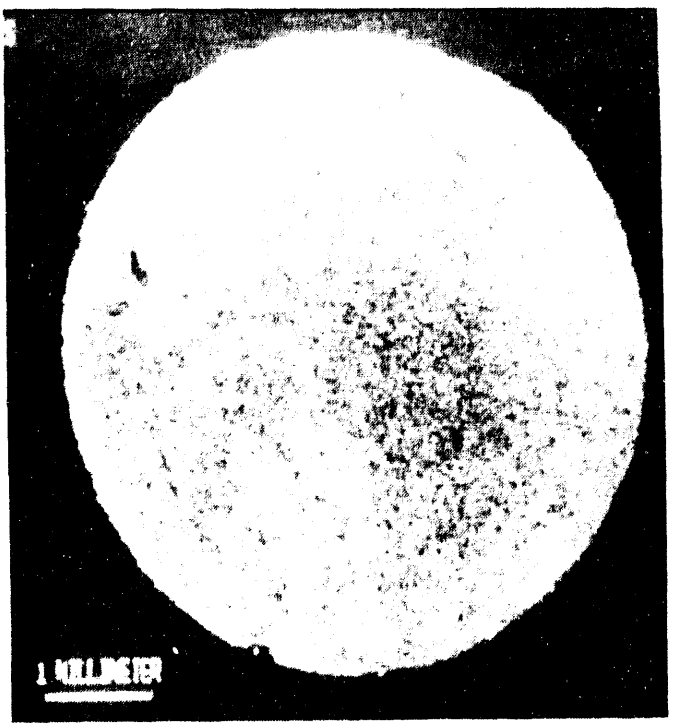

Figure 9. Zinc Ferrite Test 74
Sulfur Map

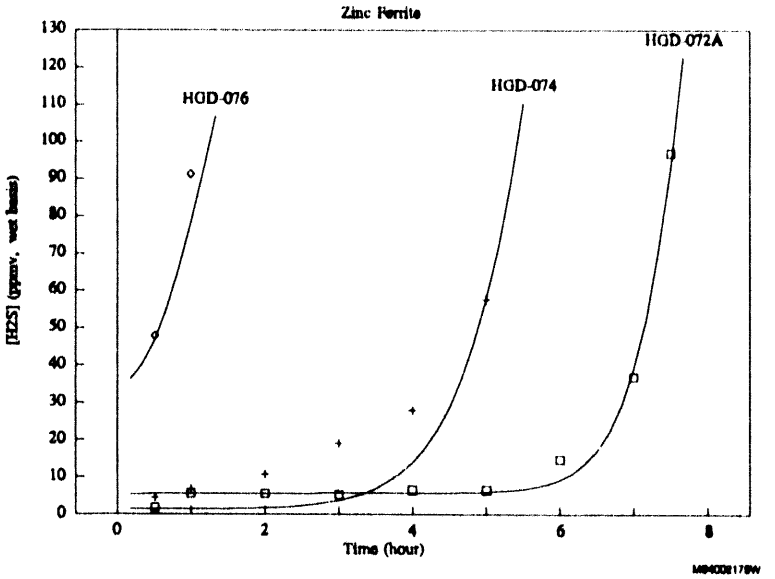

Figure 10. Breakthrough Curves

REFERENCES

Focht, et al., 1986, *Structural Property Changes in Metal Oxide Hot Coal Gas Desulfurization Sorbents*, Report No. DOE/MC/21166-2163, National Technical Information Service, Springfield, Virginia.

Grindley, T., 1982, Development and Testing of Regenerable Hot Coal Gas Desulfurization Sorbents, in *Proceedings of the Second Annual Contractors Meeting on Contaminant Control in Hot Coal Derived Gas Streams*, Report No. DOE/METC/82-47, National Technical Information Service, Springfield, Virginia.

Grindley, T., 1988, Sidestream Zinc Ferrite Regeneration Tests: Laboratory-Scale Study of Reductive Regeneration of Zinc Ferrite Sorbents, in *Proceedings of the Eighth Annual Gasification and Gas Stream Cleanup Systems Contractors Review Meeting*, Report No. DOE/METC-88/6092, National Technical Information Service, Springfield, Virginia.

Grindley, T., 1990, Effect of Chlorine on Hot Gas Desulfurization Sorbents, in *Proceedings of the Tenth Annual Gasification and Gas Stream Cleanup Systems Contractors Review Meeting*, Report No. DOE/METC-90/6115, National Technical Information Service, Springfield, Virginia.

Grindley, T., 1991, Lab-Scale Sorbent Development, in *Proceedings of the Eleventh Annual Gasification and Gas Stream Cleanup Systems Contractors Review Meeting*, Report No. DOE/METC/91-6123, National Technical Information Service, Springfield, Virginia.

Wang, et al., 1988, *Dynamic Simulation Models for High-Temperature Desulfurization Processes*, Report No. DOE/MC/23089-2601, National Technical Information Service, Springfield, Virginia.

TGRIND\7:940606

P16

High Temperature Hydrogen Sulfide Removal with Stannic Oxide

Contract Number	DE-FG03-90ER80998
Contractor	TDA Research, Inc. 12345 West 52nd Avenue Wheat Ridge, Colorado 80033 (303) 422-7830
Contractor Project Manager	Michael E. Karpuk
Principal Investigators	Robert J. Copeland (P.I.), D. Feinberg, D. Wickham, B. Windecker and J. Yu
METC Project Manager	Ron Staubly
Period of Performance	May 23, 1991 to July 31, 1994

FY94 Program Schedule

	S	O	N	D	J	F	M	A	M	J	J	A
Multiple Cycles on Single Sorbent	———											
Economic Analysis		———										
Integrated SnO_2/ZnO Experiment				—						———		

OBJECTIVES

This Phase II SBIR contract is developing a sorbent and process that removes H_2S from hot gasified coal and generates sulfur during regeneration of the sorbent. The process can be used with any type of reactor (*e.g.*, fixed or moving bed) and any gasifier (*e.g.*, KRW or Texaco) and shows lower costs than competing H_2S removal processes.

TDA Research's (TDA) process uses a regenerable stannic oxide-based (SnO_2) sorbent as the first sorbent and zinc ferrite (or zinc titanate) as a second sorbent to remove H_2S to very low concentrations. The process converts the sulfides from both sorbents to elemental sulfur, a commercial product that is easy to store and transport. The goal of this phase is to develop chemically active, high sulfur loadings, and durable stannic oxide sorbents and to demonstrate the process at the bench scale.

BACKGROUND INFORMATION

Low-cost and high-efficiency processes for the removal of sulfur compounds are required to economically apply Gasifier Combined Cycle (GCC) technology to the generation of electric power. Many commercial processes are available to remove sulfur from cold gas streams; however, cooling the gas stream reduces the overall plant efficiency. Hot gas cleanup is being developed to solve that problem; zinc oxide based sorbents effectively remove H_2S to low levels but require either land-filling or additional processing to convert the products of regeneration to a commercial item. TDA is evaluating a regenerable hot gas absorbent that will produce elemental sulfur directly during regeneration.

Elemental sulfur is the only product leaving the plant (*i.e.*, no landfill or sulfuric acid). Elemental sulfur is a dense solid that is not toxic or corrosive. Sulfur is easy to both store and transport long distances and requires less than one third of the weight and volume as the same sulfur in the form of sulfuric acid. Unless the end use of the sulfuric acid is nearby, elemental sulfur is clearly the most desirable commercial end product from the hot gas cleanup.

Process Reactions

The system is based on the absorption of hydrogen sulfide (H_2S) by stannic (tin) oxide. Two sorbents are required, the first sorbent is tin (stannic) oxide, which removes half of the sulfur. The second sorbent is a zinc oxide based material (*i.e.*, zinc ferrite or zinc titanate) that removes the other half of the sulfur from the gasified coal. The zinc oxide second sorbent reduces the sulfur of the coal gases to the low levels required by GCC. The second sorbent (*i.e.*, ZnO based) is regenerated by air producing SO_2.

TDA's process carries out a modified Claus reaction to reduce the SO_2 from the second sorbent generation to elemental sulfur. In this case the sulfided stannic oxide forms stannous sulfide (SnS), which reduces the SO_2. The reactions in the process are:

Absorption

$$SnO_2 + H_2 + H_2S \rightarrow SnS + 2\ H_2O$$
$$ZnO + H_2S \rightarrow ZnS + H_2O$$

Regeneration

$$ZnS + 1.5\ O_2 \rightarrow ZnO + SO_2$$
$$SnS + SO_2 \rightarrow SnO_2 + S_2$$

The absorption by SnO_2 could remove over 90% of the H_2S from typical coal gas streams, but we use zinc ferrite (or zinc titanate), a) to reduce H_2S to less than 20 ppm and b) as a source of SO_2 in regeneration. Due to stoichiometry of the regeneration reactions, we remove half of the H_2S by SnO_2 and the remainder by the second sorbent.

Figure 1 illustrates the process using fixed bed reactors. The H_2S containing coal gases leave the gasifier and flow first through the stannic oxide and then the zinc ferrite; both materials are contained in the same pressure vessel. During regeneration, the flow direction reverses. Air and steam flow first through the zinc ferrite, oxidizing the sulfide to SO_2. The sulfur dioxide produced by regenerating the second sorbent flows over the SnS regenerating SnO_2.

When there is both steam and SO_2 present, two regeneration reactions occur simultaneously:

$$SnS + SO_2 \rightarrow SnO_2 + S_2$$
$$SnS + 2\ H_2O \rightarrow SnO_2 + H_2 + H_2S$$

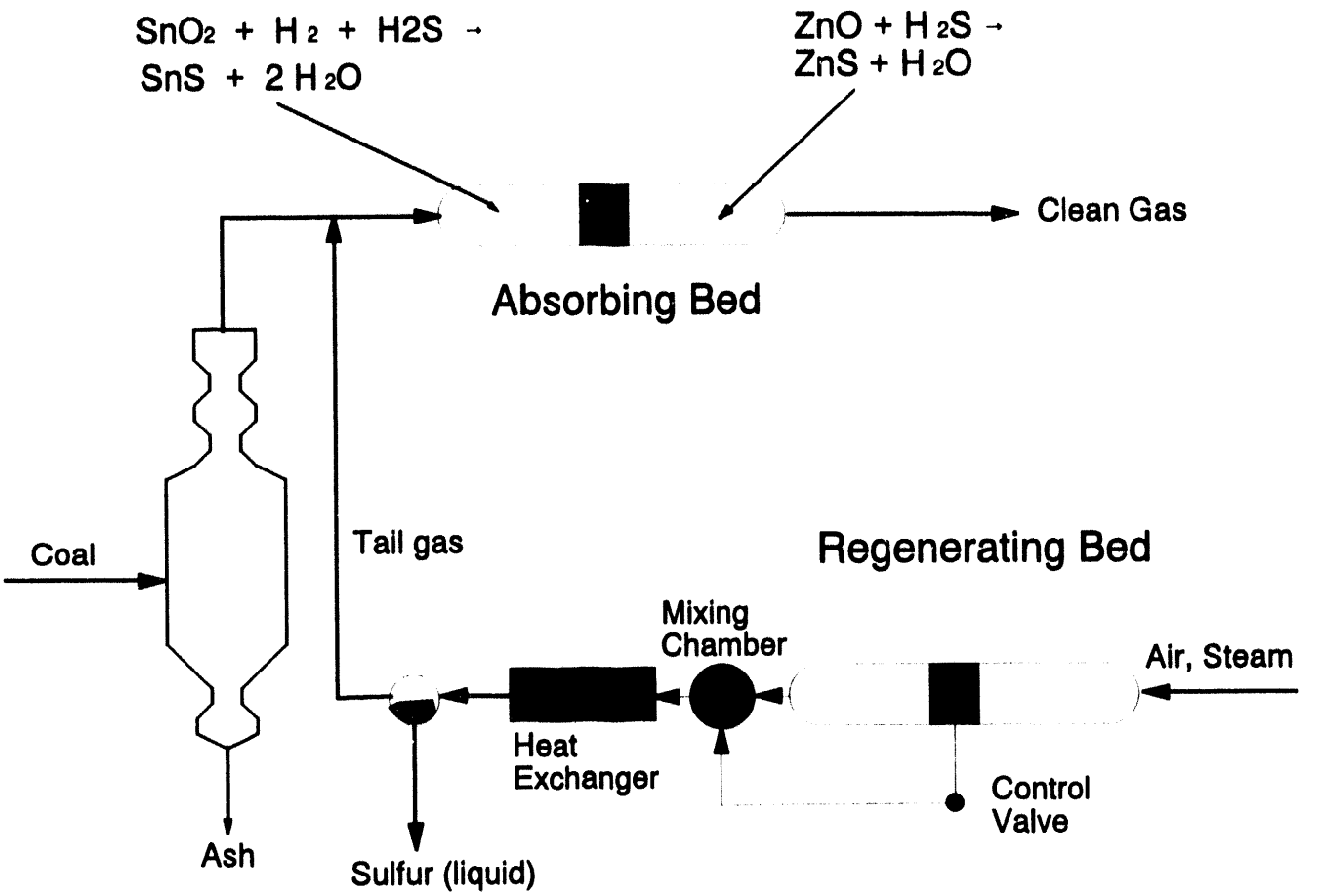

Figure 1. SnO_2 fixed bed system

One reaction produces sulfur and the second produces H_2S. We have measured the presence of both sulfur and H_2S when SnS is regenerated with a mixture of steam and SO_2. The proportion of each that is present depends on the time history of the regeneration half cycle. Early in the regeneration, H_2S is the primary product. Later in the regeneration of the fixed bed reactor, the quantity of SnS is reduced and some of the SO_2 passes through the bed. Near the end of regeneration, the H_2 and H_2S from the reaction of H_2O and SnS react with the SO_2 and sulfur is the primary product of regeneration.

The control valve shown in Figure 1 directs some of the SO_2 around the SnS portion bed. The quantity of flow diverted around the SnS varies with time. Thus, control valve maintains a stoichiometric mixture of 2 H_2S and 1 SO_2 to produce sulfur by the Claus reaction:

$$2\ H_2S + SO_2 \rightarrow 2\ H_2O + 1.5\ S_2$$

Since the gases exit the SnO_2 and ZnO beds at 700°C (1292°F), the Claus reaction in a small mixing chamber is very rapid. Cooling the mixed gases then condenses the sulfur. The sulfur condenses (but not the steam) and flows out of the system as a liquid. Un-reacted H_2O (steam), N_2, and H_2S (*i.e.*, tail gas) mixes with the gasifier outlet. The H_2S in the tail gas is then re-absorbed by the SnO_2 and/or ZnO and is ultimately removed as elemental sulfur.

The mixing of the tail gas with the gasifier outlet serves three functions simultaneously. First it cleans up the tail gas without the need for additional processing equipment. Second the cool tail gases reduce the temperature of the gasifier outlet, avoiding the need to add water to cool the gas stream down to the hot gas cleanup equipment (571°C, 1060°F). The third function is to change to composition of the gasifier outlet to one that will not reduce the stannic oxide to the metallic tin. Some gasifiers (*e.g.*, Lurgi) will not reduce stannic oxide; others (*e.g.*, KRW, Texaco) will reduce stannic oxide at high temperature. Using the steam required to control temperatures during the ZnO regeneration can also control the temperature and composition of the gas entering the hot gas cleanup system.

When this steam is already needed to control temperatures during the zinc titanate regeneration, there is no penalty in its use to control the temperature and pressure of the coal gases entering the hot gas cleanup. This dual use of steam (to cool the gasifier outlet using the steam from the ZnO sorbent regeneration) is unique to TDA's stannic oxide based process.

Regeneration Approaches

Different approaches can regenerate the stannic oxide based sorbent. We call these two approaches *high steam*, *low steam*, and *no air*. The *high steam* option is shown in Figure 1 for a fixed bed reactor but can be used with any type of reactor (*e.g.*, moving bed, fluidized bed). The *low steam* regeneration would be used with a moving, fluidized, or entrained bed. The third type using *no air* (*i.e.*, only steam) has been proposed by Nielsen *et al.* (1991) to regenerate stannic oxide from the sulfided material and reclaiming some hydrogen.

The *high steam* composition simulates a 6.5:1 steam to air ratio entering the sulfided zinc oxide based second sorbent. The regenerative gas contains 1.88% SO_2, 87.5% H_2O, and the balance N_2. This gas composition leaves the ZnO at 700°C (1292°F) due to the heat released by oxidation of the ZnS. This gas regenerates the stannous sulfide completely. Figure 1 illustrates the fixed bed system and the reactions that occur. As the SnS is regenerated initially the outlet is very high in H_2S. Some of the gases leaving the second sorbent regeneration (*i.e.*, high is SO_2) are by-passed around the SnS to the mixing chamber. The H_2S leaving the tin portion and the SO_2 leaving the zinc portion of the bed react producing elemental sulfur by the Claus reaction.

The *low steam* regeneration of the zinc oxide second sorbent is associated with a moving bed (see Figure 2) or fluidized bed reactor. This type of reactor recycles nitrogen and SO_2 to produce a high concentration of SO_2. Gal *et al.* (1992) produced SO_2 concentration as high as 10%. Our *low steam* regeneration is less demanding and requires only ≈ 3% SO_2 leaving the zinc oxide second sorbent regeneration.

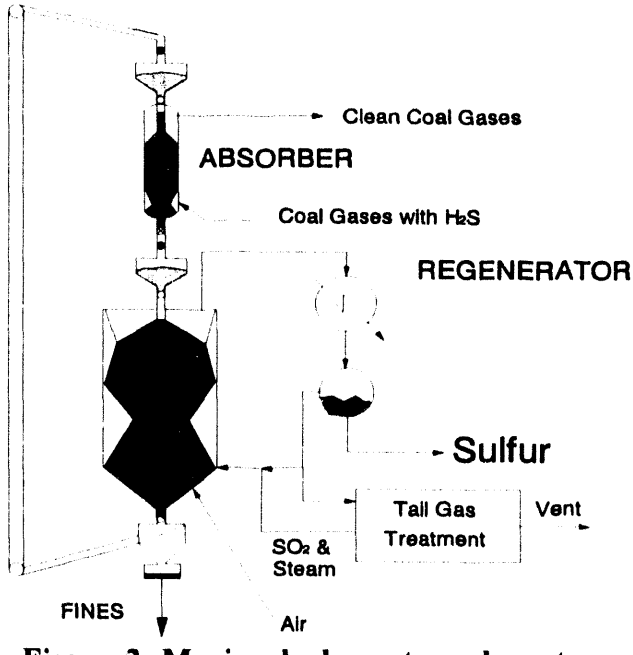

Figure 2. Moving bed reactors; low steam

In Figure 2 the sorbents are regenerated at low pressure. In that case the tail gases can not be returned to the high pressure gasified coal. The tail gases are treated (*e.g.*, SO_2 readily dissolves in water separating it from the N_2, which is then vented to the atmosphere). Heating the solution recovers SO_2 and reconditions the water. Some steam and the SO_2 steam are returned to the regeneration reactor that converts the SO_2 to sulfur.

If the regeneration is conducted at high pressure, the tail gases from the *low steam* reactors could be used to cool the gasifier outlet as in the *high steam* case. TDA's experiments utilize the *high steam* generation in most cases. We have conducted experiments with both *high steam* and *low steam* regeneration approaches and found complete regeneration of the sorbent with either approach.

The *no air* approach is described by Nielsen *et al.* (1991) using SnO_2 as the H_2S sorbent; they regenerate the SnO_2 by reversing the absorption reaction. That process uses super-heated steam [350 psia - 23.8 atm, 842°F - 450°C; 30 to 50 moles H_2O per mole of H_2S]. The steam is condensed and then a stripper solution separates the H_2 and returns it to the gasifier outlet. The concentrated H_2S is then converted to elemental sulfur in a conventional Claus plant. TDA has independently verified that the SnS can be regenerated by steam alone. However, the steam required by that process is substantially greater than both the high steam and low processes described above, thus the *no air* approach adversely affects power plant efficiency.

PROJECT DESCRIPTION

Phase II focuses on the demonstration of the process with fixed bed rectors. The fixed bed is readily scalable to small sizes, which minimizes the cost of the experiments. Sorbents suitable to moving beds could be produced by modifying the shape of the sorbent to rounded ends to improve attrition resistance. Smaller, rounded particles would be needed for fluidized or entrained bed reactors. TDA has also produced small sorbent particles suitable for fluidized and/or entrained bed reactors, but those sorbents have not been tested to date.

The key to the economic success of the proposed system is the development of a sorbent/support combination that retains its properties through multiple full absorption-regeneration cycles. These sorbents are screened for physical properties, chemical reactivity, and durability. Based on previous work in zinc ferrite and zinc titanate, TDA identified those properties that make a good hot gas cleanup sorbent.

TDA has produced >200 sorbents using different binders, different quantities of binders, firing temperatures, sources of stannic oxide, water content, forming pressure, forming technique (press, agglomerate, and extrude), and techniques for controlling pore size and porosity. Several methods of preparing the sorbent were investigated including mixed metal oxides, adding sorbent to a catalyst support.

The catalyst support method physically separates the structural and chemical requirements for the sorbent. An inert material (*e.g.*, alumina) forms the structure and the stannic oxide absorbs the H_2S. The support is first extruded and fired; then an aqueous solution of the chemical salt (*i.e.*, $SnSO_4$) is deposited on the support and decomposed. The supported catalyst approach produces a sorbent with high strength and long life but typically has low loadings and is expensive to produce.

TDA also developed a new method of producing hot gas cleanup sorbents. This new

method called a "geode" mimics the catalyst support approach, but the geode is made like a mixed metal oxide. The geode has the strength and durability of the supported catalyst but the high chemical content and low production costs of mixed metal oxides.

Geodes are naturally occurring rocks with a hollow interior; our approach was to make the geode with a porous, inert shell and to fill the interior with the chemically active stannic oxide]. We formed geodes by extrusion, pressing, and agglomeration. The best geodes were made by extrusion. We premix the inert binder material (*e.g.*, bentonite) and the stannic oxide. We then press or extrude the mixture only once and fire once to produce the geode. The geode is formed **without** decomposition of salt and **no** aqueous solution is needed anywhere in the process (*versus* a supported catalyst sorbent that requires an aqueous solution of a decomposable salt). The geode sorbent has high strength, high surface area, and high stannic oxide content (e.g. 67%, wt.).

RESULTS

Last year (Copeland *et al.* 1993) we reported on the screening of the sorbents. We identified several formulations that will meet all of our goals; and we selected one that had the best characteristics for a multiple cycle test of its properties. The selected sorbent was the geode, JY0121-1; a second batch was made after initial screening and is identified as BW0121-1. A third batch was extruded for TDA by AMAX and is identified as AX0121-1. Our most extensively tested geode is BW0121-1 and contains 67% SnO_2 by weight in the fired material; the inert is also a low cost material (bentonite). This paper describes the results of the multiple cycle testing on that geode.

Experimental Apparatus

TDA designed the experimental test apparatus to automatically cycle between absorption and regeneration while unattended. We use computer control 1) to sequence between absorption and regeneration, 2) to control all flow rates, 3) to automatically control the temperatures in the reactors, lines, boilers, and heaters and 4) to shut down the experiment in case of an emergency. The high degree of automation allows continuous operation, and we operate the system 24 hours per day.

The experimental apparatus delivers a controlled flow of mixed gases to a high pressure reactor to simulate either absorption or regeneration. The reactor is a 3.0" (O.D.) stainless steel tube that is designed for 300 psig and 1292°F (700°C). The isothermal zone of the reactor is 10" (254 mm) high with a 2.5" (6.4 mm) (I.D.). Without channelling in the bed we can tests pellets up to 0.25" (63.5 mm) in diameter with our current system.

Figure 3 illustrates the overall layout of the apparatus. A series of mass flow controllers meters the desired gas composition into the reactor. Cylinders of N_2, CO_2, CO, and H_2 are stored in the room. H_2S and SO_2 are stored in separate hoods and flow controllers supply the gases to the reactor that is inside a third hood. Water is stored in a drum and pumped into the vent hood where it is boiled and mixed with the bottle gas supply.

Two computers control and measure data for the experiments. The computer also monitors the alarms and high temperatures and shuts the experiment down if any factor (*e.g.*, high H_2S levels) exceeds preset limits. One computer controls the temperatures, flow rates, and sequences automatically between absorption and regeneration. The second computer controls the gas chromatograph and records the data from FPD and TCD detectors.

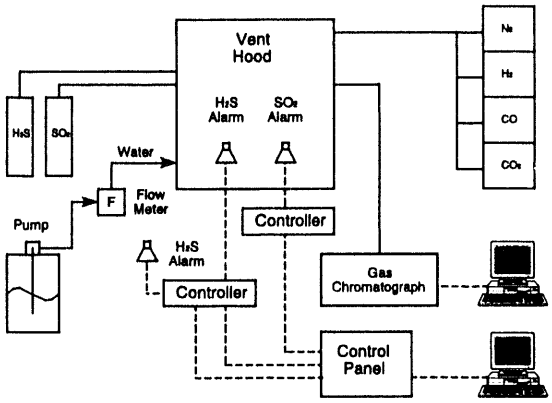

Figure 3. Schematic of experimental apparatus

We perform cycling tests simulating the inlet of a fixed bed. This location will have the highest loading of sulfur during absorption. Previous work on zinc titanate (Jung *et al.* 1992) has shown that high sulfur loadings reduce the strength of the pellets and cause failure of the sorbent. Thus, the crush strength on pellets tested under these conditions will be lowest and the most severe expected in service. The experiments are performed at high temperature. We sulfide at 1,060°F (571°C) with simulated KRW and Texaco gasifier coal gas streams and regenerate at 1,292°F (700°C) simulating both the temperature and composition of the ZnO based second sorbent outlet gas.

The experiments also evaluate the sorbent at conditions simulating the entire bed (*i.e.*, breakthrough curves). Hot gas cleanup reactors normally operate at space velocities in the range of 1500 to 2000 h^{-1}; but there are two sorbents in our bed (SnO_2 and ZnO). Since each sorbent must remove half of the H_2S, we operate the stannic oxide bed at a space velocity of 3000 to 4000 h^{-1} (ntp), which is about twice the total.

Sulfur Loading with Multiple Cycling

Two sulfur loadings are reported: the loading where the sorbent removed half of the H_2S from the inlet with a SV of 3400 h^{-1} (breakthrough) and the second loading after five hours of exposure to 1% H_2S in the inlet gas (full load).

We have measured the breakthrough sulfur loading at periodic intervals in an isothermal (1058°F) 570°C reactor. The loading has slowly declined with cycling from 4.5% sulfur at cycle 11, to 4.1% at cycle 37, and somewhat lower at cycle 64. During cycles 64 and 65 we had a boiler problem that allowed liquid water into the reactor (not steam as in previous runs) and caused the bed to be non-isothermal. Cycle 64 operated between 470 and 570°C and absorbed 3.0% sulfur. During cycle 65 the temperature was controlled to 573°C inside the reactor and the oven temperature was 727°C; under these conditions the BW0121-1 absorbed 8.4% sulfur and removed 78% of the H_2S. If the test had been continued to the point where 50% of the sulfur was removed by the stannic oxide, the sulfur loading would have been higher.

We also measured the sulfur loading after 5 hours of exposure to 1% H_2S with an isothermal 1058°F (570°C) reactor. The loading has slowly declined with cycling from 7.7% sulfur at cycle 11, to 5.7% at cycle 37, and noticeably lower at cycle 64. During cycle 64 and 65 we had a boiler problem and a non-isothermal reactor. Cycle 64 operated between 878°F and 1058°F (470 and 570°C) and absorbed 3.1% sulfur. During cycle 65 the temperature was 1063°F (573°C) inside the reactor and the oven temperature was 1341°F (727°C); under these conditions the BW0121-1 absorbed 8.4% sulfur.

Crush Strength & Mass Losses

Periodically, the pellets were removed from the reactor and the remaining mass of whole pellets was weighed. Some whole pellets were removed and analyzed for the properties of the sorbent (*i.e.*, crush strength). The remaining pellets were again weighed before returning them to the reactor. The properties of the BW0121-1 with cycling are given in Table I.

Table I. Cycling effects on crush strength and mass loss

Cycle Number	Crush Strength lb/mm	Mass Loss Rate %/cycle
initial	4.6	-
2 regenerated	-	0.33
10 regenerated	5.3	0.35
22 regenerated	6.2	0.35
36 regenerated	4.3[1]	0.92[1]
43 regenerated	_	0.008
63 sulfided	5.7	0.469

[1] At end of 36th cycle, cooling of the reactor caused all of the pellets in the reactor to be flooded with water; the rapid cooling associated with a water quench would not be experienced in practice. This quench may have weakened some pellets or caused fracturing with others.

The weight of the material that was removed from the reactor is subtracted from that which was added to calculate the loss of material. By dividing by the number of cycles, the average loss per cycle is then calculated (*i.e.*, the reciprocal of the cycle life) during each period.

We subtracted the mass of pellets that are used for sample taking and fitted a curve to the experimental data; Figure 4 illustrates the curve fit to the data. The average loss of material through 63 cycles is 0.476%/cycle implying a cycle life of 210 cycles.

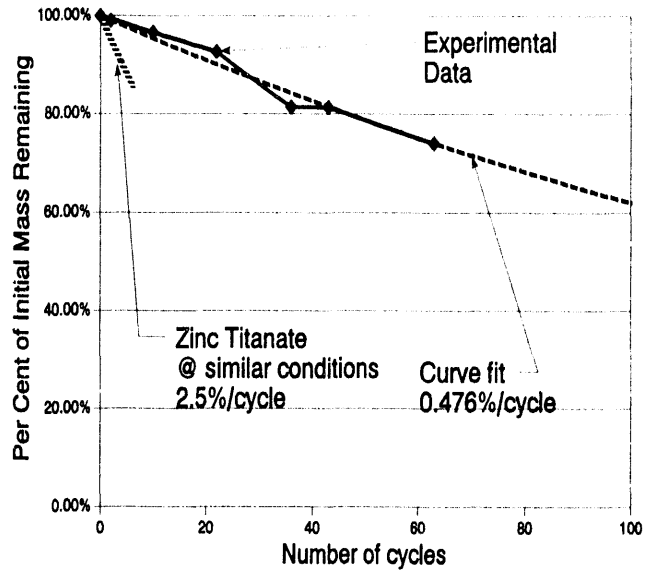

Figure 4. Effect of cycling on BW0121-1

The loss rates for a zinc titanate sorbent is also shown in Figure 4; the data are for TRZ-21 as reported by Jung *et al.* (1992). Both the stannic oxide and the zinc titanate sorbents were tested under simulated inlet conditions and the zinc titanate is rapidly destroyed under these conditions (2.5% mass loss per cycle). By comparison, the stannic oxide sorbent losses were very low (0.476%/cycle), which is a direct result of the way we make our sorbent and the properties of stannic oxide.

These experiments tested pellets that are at the inlet of a fixed bed reactor. At that condition the sulfur loading is the highest, creating the greatest changes in the chemical sorbent and the greatest stresses on the sorbent. However, the bed average sulfur loading would be smaller than these test conditions, the life of a whole pellet would be greater than the pellets that are at the

inlet (over 300 cycles for the bed average conditions is anticipated).

Surface Area

We measured the surface area of the materials regeneration sorbent with our BET apparatus. Table II presents the measured surface area of three batches of sorbents with the same formulation. The JY0121-1, BW0121-1, and AX0121-1 are chemically the same (but the AX0121-1 was extruded, the other two were different batches of pressed pellets). There is a loss of surface area with cycling and this roughly correlates with the loss of sulfur capacity with cycling.

Table II. Effect of cycling on surface area

Cycle Number	State	Surface Area: m^2/g
Initial Sorbent JY0121-1 AX0121-1	SnO_2	 3.9 4.5
Tenth JY0121-1 BW0121-1	SnO_2	 2.0 1.0
22nd BW0121-1	SnO_2	0.7
36th BW0121-1	SnO_2	0.6
63rd BW0121-1	SnS (SnO_2)	 1.7

The surface area for the BW0121-1 for cycle 63 was higher than all but the initial surface area for this sorbent. This sample was removed from the reactor in the sulfided state, and then regenerated in the oven at 1292°F (700°C). The high surface area may be due to the more rapid regeneration of the stannic oxide when oxidized by air *versus* SO_2-H_2O in the previous cycling. If that is true, surface area (and probably sulfur capacity) could be periodically recovered by air regenerating the sorbent.

Breakthrough Characteristics of SnO_2 Sorbent

Figure 5 presents the breakthrough characteristics of the SnO_2 sorbent. The bed contains BW0121-1 (same as JY0121-1, but a different batch) with a bed of 387 g occupying 256 cc. The simulated KRW gas stream flows at Space Velocity (SV) of 3400 h^{-1} and its pressure is 130 psia (8.85 atm). The inlet H_2S concentration was 9962 ppm (v) and set higher than a KRW gasifier's concentration to minimize the duration of the test. For a short time the concentration is around 800 ppm, indicating >90% removal of the H_2S. As the bed loads with sulfur the exit concentration rises rapidly at first, and then slowly.

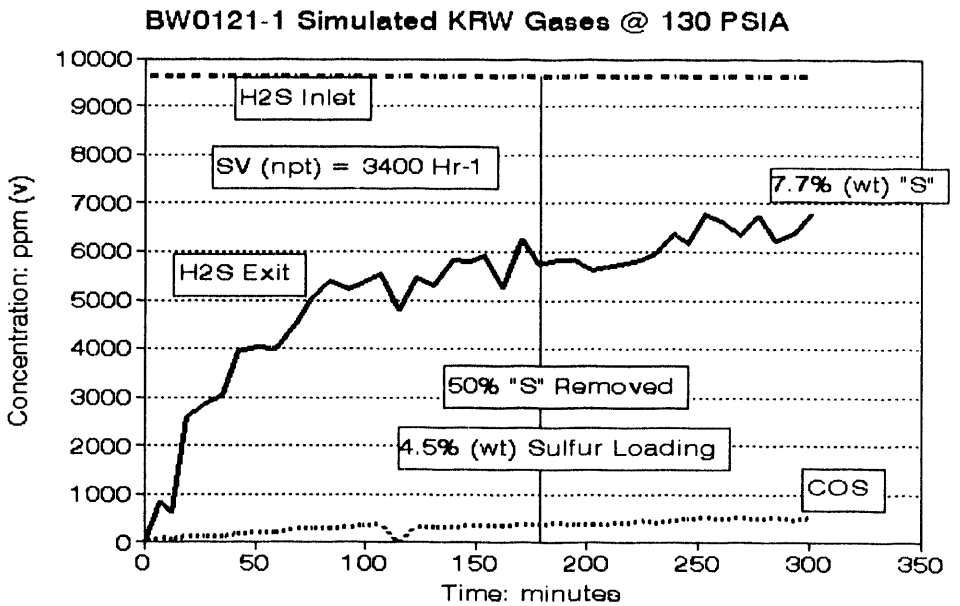

Figure 5. Breakthrough characteristics: 11th absorption cycle (570°C)

Figure 6 presents the breakthrough curve for absorption cycle number 37 on the BW0121-1 pellets. In comparison to the breakthrough curve for cycle number 11, the loading of the pellets decreased slightly to 4.1% from 4.5% (sulfur by weight). Breakthrough came at approximately the same time as in cycle number 11.

As shown in Figure 6 the pellets were not completely regenerated at the start. At time=0 minutes, we added H_2S and continued the flow for 5 hours. As in the previously data (Figure 5, cycle 11) the H_2S outlet increased rapidly and slowly with time.

The breakthrough characteristic for cycle 65 is shown in Figure 7 with simulated KRW gases. A very low H_2S concentration was sustained for a long period of time. The calculated sulfur loading was 8.4%. The data demonstrate that very high loadings can be achieved with this material in high temperature use, even after many previous cycles have been accumulated on the same batch of pellets. Following the 65th absorption we prepared to regenerated the sorbent. Unfortunately we experience a temperature excursion in our electrically heated tube furnace. The temperature exceeded 1832°F (1000°C) for a time. Since the melting point of SnS is 1918°F (881°C) and most of the tin was sulfided, the pellets melted and were destroyed. No addition cycling was possible with the BW0121-1 pellets.

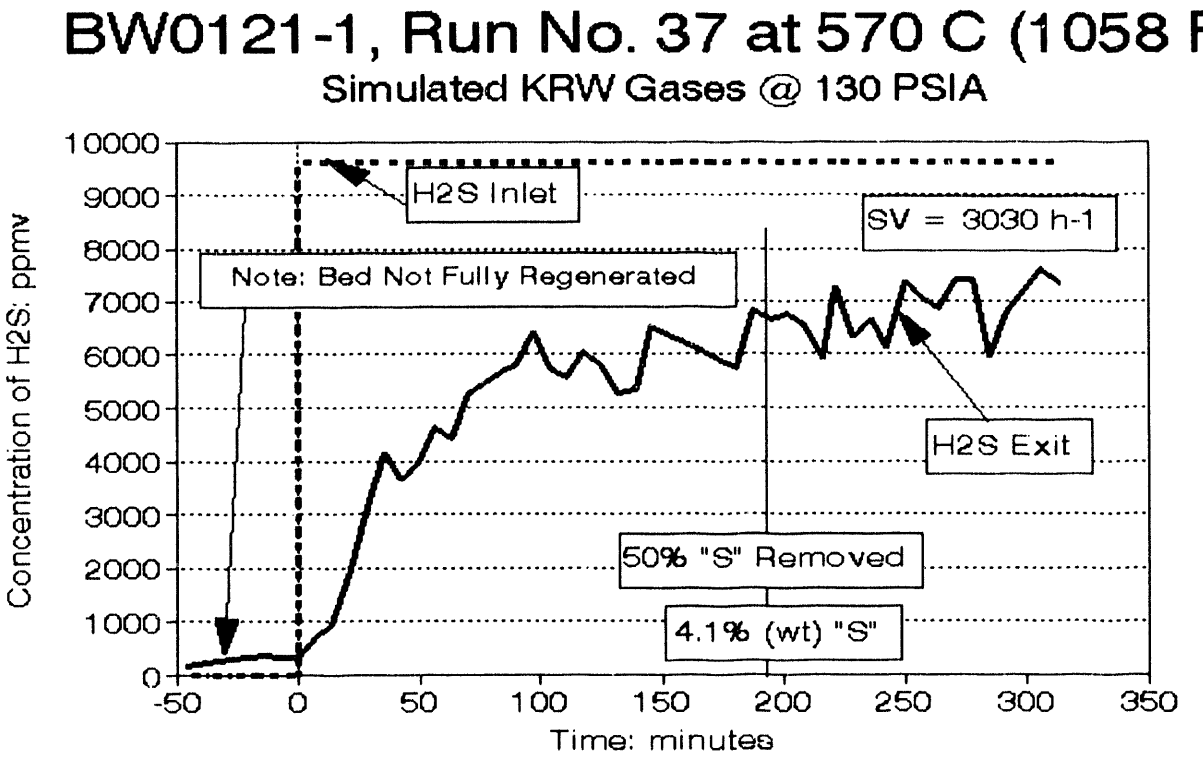

Figure 6. Breakthrough characteristics: 37th absorption cycle (570°C)

The high loading on cycle 65 was a direct result of the high temperature of the sorbent (570 to 727°C). We independently conducted experiments with another geode, BW0121-3 and measured its sulfur loading as a function of temperature. We found a very strong correlation with low temperatures absorbing low quantities of sulfur and high temperatures absorbing more.

Refabrication of Sorbent

An economical sorbent must have significant life at an affordable cost. The cost of SnO_2 is ≈ $5/lb; even with a life of 200 cycles the operating cost of the system would be high, if the stannic oxide were thrown away after a number of cycles. To avoid this problem TDA defined a tin recovery system to reclaim the tin from the spent sorbent. This system is illustrated in Figure 8 for a moving bed reactor. The recovery and reuse of the tin increases the effective cycle life (*e.g.*, > 4000 cycles with 95% recovery of the tin in each refabrication).

The moving bed reactors operate in the same manner as the reactors described by Cook *et al.* (1991). In this system the stannic oxide and zinc ferrite are mixed together (either as separately produced sorbents or combined in one sorbent). Both sorbents enter the top of the absorber, and the reaction with H_2S converts both the stannic oxide and zinc ferrite to sulfides. The same chemical reactions occur in the moving bed as in the fixed bed system. The tin recovery unit recovers the stannic oxide from sorbent fines.

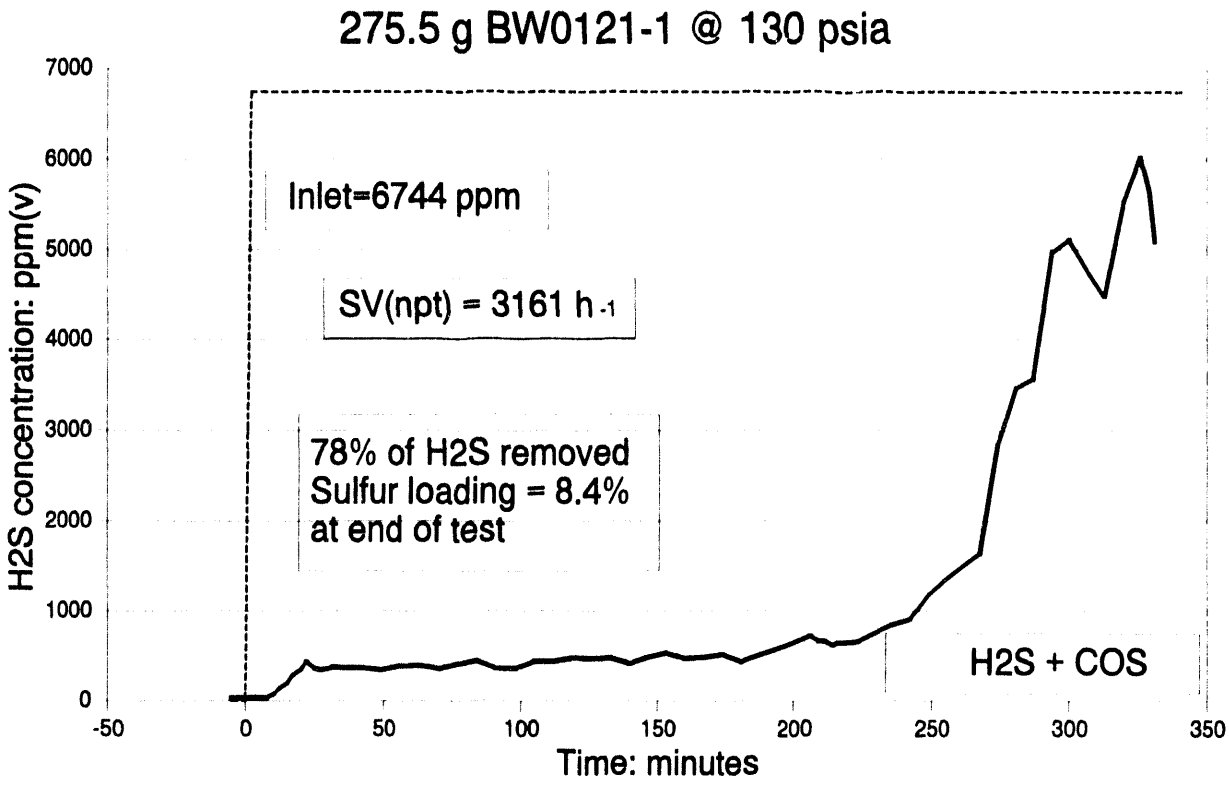

Figure 7. Breakthrough characteristics: 65th absorption cycle (570-727°C)

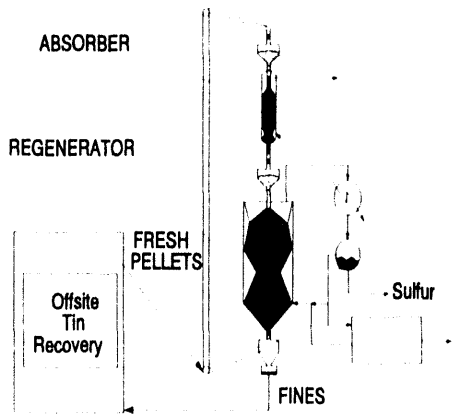

Figure 8. Tin recovery system

The recovered material is then made into fresh pellets that are returned to the moving bed reactors (or fixed bed or fluidized bed reactor).

TDA estimated the cost to produce stannic oxide pellets for IGCC power plants. We designed a conceptual pellet fabrication plant to service 500 MW_e power plants In this analysis we assume that SnO_2 removes half of the sulfur with a pellet sulfur loading of 4% by weight and a pellet life of 100 cycles. 5,778 tons/year of replacement pellets are required when operated on high sulfur coal (Illinois No. 6).

Each power plant will require an initial inventory of 2,889 tons of new BW0121-1 pellets (*i.e.*, 67% SnO_2 by weight). The quantity of pellets is large to provide a six month inventory of materials. This inventory is divided into several uses: 1) active material in the reactors absorbing H_2S, 2) spent sorbent awaiting shipment to the refabrication plant, 3) fresh pellets stored on site awaiting loading into the

to operate our system in that gasifier plant and operated it with high sulfur, Illinois No. 6 coal.

Figure 9 presents a comparison of the levelized electricity cost for four hot gas cleanup systems. Our stannic oxide process offers the lowest cost electricity when a nominal shipping cost is included. (Based on a price quote for shipping sulfur and sulfuric acid from Denver to Salt Lake City in Jumbo railway cars from a Union Pacific station to a Union Pacific station.) Shipping sulfur is much less expensive than sulfuric acid, since H_2SO_4 weighs about three times as much as an equivalent quantity of sulfur.

If users for the sulfuric acid are nearby and the operator wishes to market the sulfuric acid, then shipping would not be significant; in that case GE's process produces electricity at a cost slightly less than our process. Since the sulfuric acid process produces more usable heat (*i.e.*, the sulfur is burned to SO_2) and three times as much product at a similar selling price per ton, those factors generate more revenue for the sulfuric acid plant than selling sulfur. The higher revenues more than pay for its operating and capital cost (*i.e.*, producing sulfuric acid is a profitable business). Of course if the utility wanted to sell sulfuric acid, it could always burn the sulfur from our process to produce the acid in an on-site or off-site sulfuric acid plant. The two plant (power and acid) operations would be completely separated. That approach increases the reliability of the overall plant, since operation of the power plant is not tied to the operation of the acid plant.

RTI's Direct Sulfur Recovery Process (DSRP) produces the same product as our system. The primary difference between our stannic oxide system and the DSRP is the efficiency. We consume 0.5 moles of H_2 or CO per mole of H_2S removed from the gas. The DSRP consumes 4.0 moles of H_2 or CO per mole of H_2S. Thus, the DSRP removes a significant

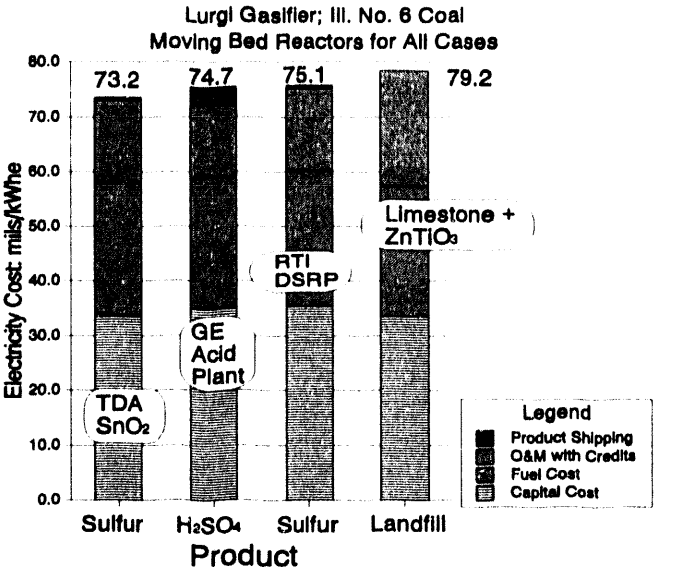

Figure 9. Comparison of electricity costs with the same gasifier and combined cycle

fraction of the heating value of the gasified coal and generates some steam for power generation with the heat that is generated. However, burning the fuel in the gas turbine is more efficient and that difference makes our process more efficient and lower cost.

The limestone + zinc titanate process has the lowest capital cost, the highest efficiency, and no product shipping cost (*i.e.*, we assumed a local landfill). However, the limestone incurs costs, landfilling adds more costs, and there is no product to sell. The operating costs are relatively high, making it the most expensive of the processes considered.

Closure

TDA has developed a new process and a long life sorbent for high temperate hydrogen sulfide removal. The economics of the process have been evaluated; the cost of electricity using the stannic oxide system is potentially the lowest cost hot gas cleanup system.

While stannic oxide is a relatively expensive material ($5/lb), spent sorbent can be refabrication into fresh sorbent. The price of the refabricated stannic oxide geode is <$2,000/ton, which is equal to or less than zinc oxide based sorbents.

REFERENCES

Chen, H.T., M.G. Klett, M.D. Rutkowski, and R. Zaharchuk (1993). "IGCC Database and Hot Gas Cleanup Systems Studies," *Proceedings of the Coal-Fired Power Systems 93 -- Advances in IGCC and PFBC Review Meeting*, sponsored by the U.S. Department of Energy, Morgantown Energy Technology Center: Morgantown, West Virginia, Report No. DOE/METC-93/6131 (CONF-9306148).

Chen, H.T., M.G. Klett, and M.D. Rutkowski (1992). "Sensitivity of Hot Gas Desulfurization on IGCC Cost of Electricity," in *Proceedings of the Twelfth Annual Gasification and Gas Stream Cleanup Systems Contractors Review Meeting*, Morgantown, WV: U.S. Department of Energy, Morgantown Energy Technology Center, Report Number DOE/METC-91/6128 (CONF-920951).

Cook, C.S., E. Gal, A.H. Furman, and R. Ayala. 1991. Integrated Operation of a Pressurized Fixed-Bed Gasifier and Hot Gas Desulfurization System. In *Proceedings of the Eleventh Annual Gasification and Gas Stream Cleanup Systems Contractors Review Meeting*, **1**, 45-55. DOE/METC-91/6123. Morgantown, WV: U.S. Department of Energy.

Copeland, R.J., D. Feinberg, B. Windecker, and J. Yu (1993) *Proceedings of the Coal-Fired Power Systems 93 -- Advances in IGCC and PFBC Review Meeting*, sponsored by the U.S. Department of Energy, Morgantown Energy Technology Center: Morgantown, West Virginia, Report No. DOE/METC-93/6131 (CONF-9306148).

Gal, E., A.H. Furman, and R. Ayala (1992). "Integrated Operation of a Pressurized Fixed Bed Gasifier and Hot Gas Desulfurization System, *Proceedings of the Twelfth Annual Gasification and Gas Stream Cleanup Systems Contractors Review Meeting*, editors R.A. Johnson and S.C. Jain, Morgantown, West Virginia: U.S. Department of Energy, Morgantown Energy Technology Center, Report No. DOE/METC-92/6128.

Heinemenn, H. and G.A. Somorjai (1992). "Catalytic Gasification Fundamentals," *Proceedings of the Twelfth Annual Gasification and Gas Stream Cleanup Systems Contractors Review Meeting*, editors R.A. Johnson and S.C. Jain, Morgantown, West Virginia: U.S. Department of Energy, Morgantown Energy Technology Center, Report No. DOE/METC-92/6128.

Jung, D.Y., J.S. Kassman, T.F. Leininger, J.K. Wolfenbarger, and P.P. Yang (1992). "Integration and Testing of Hot Desulfurization and Entrained Flow Gasification for Power Generation Systems," *Proceedings of the Twelfth Annual Gasification and Gas Stream Cleanup Systems Contractors Review Meeting*, editors R.A. Johnson and S.C. Jain, Morgantown, West Virginia: U.S. Department of Energy, Morgantown Energy Technology Center, Report No. DOE/METC-92/6128.

Nielsen, P.E.H., P. Rudbeck, and H. Christiansen (1991). "Steam Regenerable Sulfur Absorption Masses and Their Application in IGCC Plants," presented at the Tenth EPRI Conference of Coal Gasification Power Plants, San Francisco, California, October 16-18, 1991.

Ulrich, G.D. 1984. *A Guide to Chemical Engineering Process Design and Economics*. New York: John Wiley and Sons.

P17 Fossil Fuel Conversion - Measurement And Modeling

CONTRACT INFORMATION

Contract Number: DE-AC21-93MC30040

Contractor: Advanced Fuel Research, Inc.
87 Church Street
(203) 528-9806

Subcontractor:
Brigham Young University
(801) 378-4326

Contractor Program Manager: Peter R. Solomon — L. Douglas Smoot

Principal Investigators: Michael A. Serio, David G. Hamblen — B. Scott Brewster, Predrag T. Radulovic

METC Program Manager: Norman T. Holcombe

Period of Performance: September 14, 1993 to September 13, 1996

FY94 Program Schedule

		S	O	N	D	J	F	M	M	J	J	A
1.	Research Plan	———	———	———	———							
2.	Gasification Processes					———	———	———	———	———	———	———
3.	Gas Phase Combustion					———	———	———	———	———	———	———
4.	Fluidized-Bed Systems					———	———	———	———	———	———	———
5.	Applications					———	———	———	———	———	———	———

OBJECTIVES

The main objective of this program is to understand the chemical and physical mechanisms in coal conversion processes and incorporate this knowledge in computer-aided reactor engineering technology for the purposes of development, evaluation, design, scale up, simulation, control and feedstock evaluation in advanced coal conversion devices. To accomplish this objective, this program will: 1) provide critical data on the physical and chemical processes in fossil fuel gasifiers and combustors; 2) further develop a set of comprehensive codes; and 3) apply these codes to model various types of combustors and gasifiers (fixed-bed, transport reactor, and fluidized-bed for coal and gas turbines for natural gas).

BACKGROUND INFORMATION

To expand the utilization of coal, it is necessary to reduce the technical and economic

risks inherent in operating a feedstock which is highly variable and which sometimes exhibits unexpected and unwanted behavior. Reducing the risks can be achieved by establishing the technology to predict a coal's behavior in a process. This program is creating this predictive capability by merging technology developed at Advanced Fuel Research, Inc. (AFR) in predicting coal devolatilization behavior with technology developed at Brigham Young University (BYU) in comprehensive computer codes for modeling of entrained-bed and fixed-bed reactors and technology developed at the U.S. DOE-METC in comprehensive computer codes for fluidized-bed reactors. These advanced technologies will be further developed to provide: 1) a fixed-bed model capable of predicting combustion and gasification of large coal particles, 2) a transport reactor model, 3) a model for lean premixed combustion of natural gas, and 4) an improved fluidized-bed code with an advanced coal devolatilization chemistry submodel.

PROJECT DESCRIPTION

The program consists of five tasks: 1) Preparation of a Research Plan, 2) Modeling of Gasification Processes, 3) Modeling of Gas Phase Combustion, 4) Modeling of Fluidized Bed Systems, and 5) Applications. This paper describes the initial work performed during the first year of the contract.

RESULTS

Devolatilization of Large Coal Particles (AFR) - Large coal particles are typically used in fixed-bed combustion and gasification processes. The objective is to extend the Functional Group - Depolymerization, Vaporization, Crosslinking (FG-DVC) model that was developed for small coal particles to these centimeter size particles. Work is being carried out in three steps, 1) modeling heat transfer in a spherical coal particle, 2) development of a simplified coal devolatilization model based on FG-DVC, and 3) integration of the heat transfer model and the simplified coal devolatilization model.

Work started with the heat transfer model. Code development for the simplest situation with constant density, heat capacity and thermal conductivity and in the absence of pyrolysis was completed. The numerical solution is in good agreement with the analytical solution given by Jakob (1959). Future work will concentrate on integration of the FG-DVC pyrolysis model. Temperature dependent coal properties will be used in the code based on Merrick's thermal physical coal model (Merrick, 1983).

Reduced Version of Coal Devolatilization Model (AFR) - To model the devolatilization of large coal particles, it is necessary that the rate equations of coal devolatilization be appropriately expressed and solved along with the heat transfer equation. It is well known that coal devolatilization is a complicated process, and cannot easily be modeled with a single rate equation, especially when the elemental compositions of char, gas, and tar and the amounts of the individual gas species are desirable. The full FG-DVC model was implemented in the current version of the advanced fixed-bed code (FBED-1) in the previous contract, with the assumption that the particles are isothermal. Incorporating an intra-particle heat transfer model will require a substantial simplification of the FG-DVC model, in order to reduce the computational burden.

After a careful re-examination of the FG-DVC model, a number of model simplification options have been proposed. Option 1 is a single rate equation model which solves the total pyrolysis weight loss. Other time dependent variables, such as the yields of tar and gas species, are calculated by correlation with the weight loss. Option 2 has a single rate equation for total gas

yields and the DVC network submodel to predict the tar yield. Option 3 is Option 2 plus a submodel for nitrogen gas release, which cannot be evaluated accurately with the weight loss correlation due to its heating rate dependence. These options were constructed based on the following considerations:

1. Devolatilization of individual gas species occurs independently (except for NH_3, HCN) in the model.

2. Tar and gas evolution are coupled.

3. Tar evolution is influenced by pressure and heating rate. In order to model the pressure and heating rate dependence, the tar submodel in FG-DVC must be retained. However, this can be implemented in a pre-processing step so that the computational burden is not unduly increased.

It was therefore assumed that:

1. The total light gas evolution can be modeled using a single rate equation with a distributed activation energy accounting for multiple gas species contributions.

2. When the tar evolution amount is known from a pre-processing step, it can be treated as another "gas species" in addition to the light gas evolution, so the total volatile evolution can be modeled with a single rate equation.

3. Alternatively, the tar submodel can be solved along with the light gas species model, but it adds an additional computational burden.

4. The amounts of individual gas species can be recovered from correlation with the total volatile or total light gas amounts. This correlation is provided by the full FG-DVC model calculation which is run in a pre-processing step.

In summary, the light gas species can be modeled with a simplified model since these evolve independently, but the tar submodel cannot be easily simplified since the evolution depends on the process conditions (heating rate, pressure). With Option 1, the tar amount is estimated from the preprocessing step with FG-DVC based a nominal heating rate and bed pressure. Tar is then lumped into the total volatile equation and its contribution is modeled via its share in the activation energy distribution. In this case, the gas elemental composition is correlated with the total weight loss. The correlation is given by a standalone FG-DVC calculation and is an input to the one-equation model. The predictions of coal pyrolysis at a given heating rate by the one-equation model (Option 1) and by the full FG-DVC model are generally in good agreement.

Transport Reactor Modeling (AFR) - To model transport reactors, we plan to start with the entrained-bed coal gasification code developed at BYU, PCGC-2. Since transport reactors have particle loadings which are much higher than entrained-beds, dispersion of particles and their interactions with the gas phase become important. A stochastic turbulence particle dispersion model is being developed and is being verified with available data. It is also recognized that there exist fluctuations of particle number density everywhere in the reactor. A model accounting for this effect has been outlined and will be implemented into our particle model. Literature reviews for data on chemical and physical processes in transport reactors for model validation are underway.

The work during the first year was focused on developing and verifying a standalone turbulence particle dispersion model. Once it is verified, it will be implemented in PCGC-2, replacing the existing empirical particle dispersion model. The code then will be executed to convergence for transport reactor conditions which feature moderate particle loadings. This model uses the Ornstein-Uhlenbeck stochastic process to simulate the turbulent component of the gas velocity. It was demonstrated that the turbulence generated has the exact values of k and the time scale given by the k-ϵ model. This is the advantage of our model in comparison with those of Gosman and Ioannides (1981), and Shuen et al. (1983). Their models used a direct Monte Carlo method to alter the local gas velocity and these numerical schemes will not necessarily give the correct values of k and ε. There are in-depth discussions on the numerical solution of stochastic equations which use the Ornstein-Uhlenbeck process by Kloeden and Platen (1982). Truncated Fourier series with independent Guassian random coefficients were also used to simulate the gas turbulence (for example, Wang and Stock (1992)), but computing a truncated Fourier series consumes large amounts of computer time. Our model is much more efficient.

In order to verify our model, predictions of particle dispersion need to be compared with existing data. One such comparison has been made with data in grid generated turbulence by Snyder and Lumley (1971). It was found that our model under-predicts the data. Shuen et al. (1983) indicated that their model was calibrated with Snyder and Lumley's data (1971), but the nature of this calibration is not clear. We agree with Shuen et al. (1983) that it may be due to the arbitrary estimation of the time and length scales of the turbulence. It is true that, although the Eulerian integration time and length scales do present the scales in which the turbulence develops, they may not be quantitative enough to be used in the turbulence particle dispersion model. Our model is clearly limited by the state-of-the-art in understanding gas turbulence phenomenon. Although this is a fast advancing field, the k-ε description is still the most commonly accepted model. Using other turbulence models is beyond the scope of this contract and we will continue to rely on the k-ε description. In order to fit Snyder and Lumley's data (1971), the time scale given needs to be increased by a factor of 2.7. The validation of this approach needs to be proved by comparing with more data.

Work was also carried out to calculate the Eulerian particle properties, such as the mean velocity and the particle number density, from the stochastic particle model. Obtaining statistically meaningful values requires a large number of particle trajectories. The distributions of particle number density are plotted in Figures 1a and 1b with 500 and 5,000 particle trajectory calculations, respectively. The calculation was based on Snyder and Lumley's fluid data mentioned above and particles were injected from a point source up-stream. It is clear that, while the two calculations resulted in the same distributions, the distribution in Figure 1b is much smoother than that in Figure 1a. The insufficient number of trajectories which resulted in the noisy signals in Figure 1a, would cause severe convergence problem in the gas phase calculation, especially at high particle loadings. Since practical inlet pipes have finite diameters, model calculations have to inject particles from multiple positions throughout this diameter. Calculating 5,000 particle trajectories at each injection point imposes a heavy computational load on the code. We have to calculate only the number of trajectories, that is practically possible and look for ways to smooth the noisy distributions.

Fluidized-Bed Modeling (AFR) - The work on fluidized-bed modeling is directed toward developing a coal devolatilization submodel for an existing fluidized-bed code, MFIX. A simplified

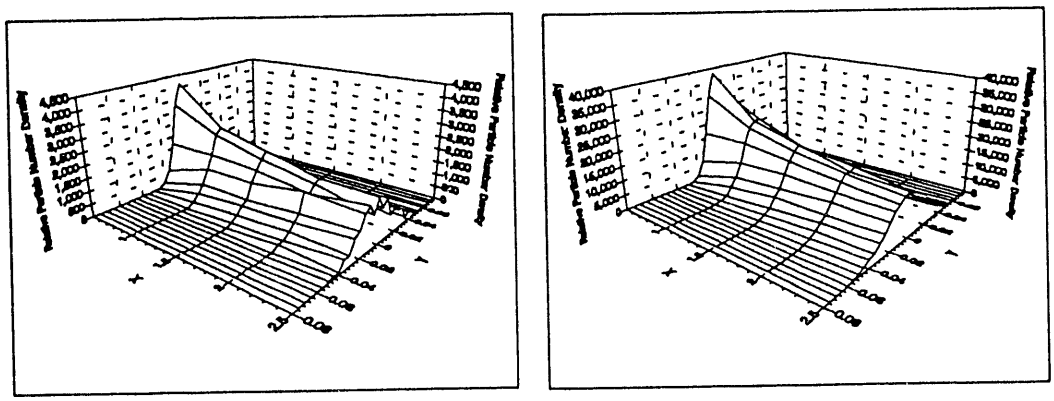

a. b.

Figure 1. Relative Particle Number Density Calculated From the Stochastic Particle Dispersion Model. Gas Fluid Data are From Snyder and Lumley (1971). a) 500 Particle Trajectories and b) 5000 Particle Trajectories.

version of FG-DVC will be tailored toward the needs of fluidized bed models. Currently, the same options for model simplification and submodel specifications that are being developed for the Fixed-Bed Reactor code are also being considered for the fluidized code.

Oxidation Rates for Large Coal particles at High Pressures (BYU) - Fixed-bed combustion and gasification processes are typically done with large coal particles at high pressures but the previously available fixed-bed codes use kinetic rates derived from small particle experiments at atmospheric pressure. Thus, work began to measure kinetic rates for large coal particles at high pressures.

A unique experimental facility was constructed to obtain oxidation rates of large particles at high temperatures and high pressures. It consists of a cantilever beam balance insert for the BYU High Pressure Controlled Profile (HPCP) reactor. The balance unit measures the mass loss of the particles as they oxidize in the HPCP reactor. It includes a force transducer, a ceramic cantilever beam, and a platinum wire-mesh sample basket. The basket is secured to the cantilever beam and extends into the reactor tube through one of the optical access ports of the HPCP reactor. This facility will permit measurements of the oxidation and gasification rates of char particles at pressures up to 17 atm and temperatures up to 1700 K. Bateman et. al., (1994a) successfully demonstrated the use of this experimental setup to study the effect of pressure on oxidation rates of mm-sized char particles. Bateman et. al., (1994b) conducted experiments with Utah bituminous and North Dakota lignite coals at 1, 5, and 7.5 atm total pressure. In these experiments, 5 and 8 mm diameter particles were used. The reactor temperature was varied between 900 and 1200 K and the bulk gas was air. Following the ignition and devolatilization stages, continuous char oxidation rates were measured to burnout. The oxidation rates were significantly increased with increased pressure but found to be independent of temperature. The effects of particle mass and pressure on the oxidation rates of a Utah bituminous char particle are shown in Figures 2 and 3, respectively. The effect of multiple particles on the oxidation rates was also studied. A pair of similarly sized individual particles of coal had similar oxidation times to a single particle having a mass equal to the sum of

the pair. The observed pressure effects could not be explained by a simple global model based on oxygen diffusion to the surface.

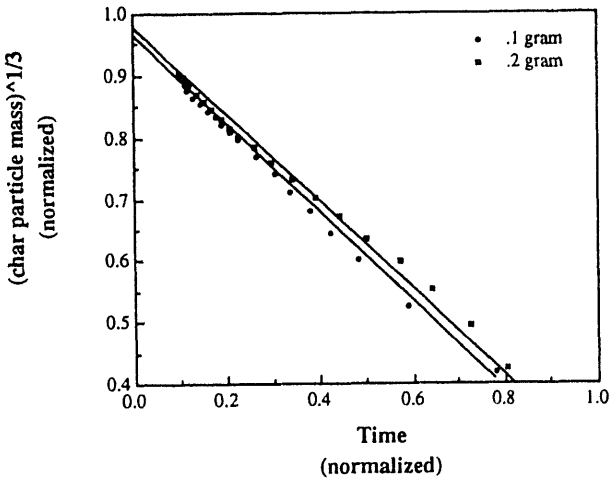

Figure 2. Normalization of the Oxidation Curve for Utah Coal, Sizes 0.1 Gram and 0.2 Gram, in the HPCP Reactor for a Gas Temperature of 900 K and an Air Flow Reynolds Number of 126 at Atmospheric Pressure.

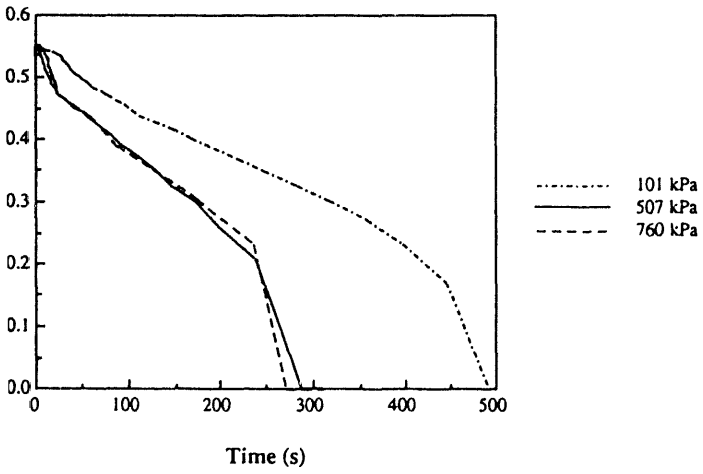

Figure 3. Comparison of Trends of 101 kPa, 507 kPa, and 760 kPa Tests for Utah Coal, Size 0.2 gram, in the HPCP Reactor for a Gas Temperature of 900 K and an Air Flow Re=126.

This study provided the first kinetic rate data for large coal particles at high pressures. The data gave significant new insights into the oxidation process regarding the temperature and pressure dependence and the role of the ash layer. The results also raised important questions: (1) What processes cause the significant effects of both temperature and pressure? (2) Why does the ash layer contract as it does during burning? (3) Why does a group of smaller particles burn like one large particle? (4) Why does the rate of burnout accelerate toward the very end of burnout? (5) Why do some low rank particles ignite before devolatilization? and (6) Why do some bituminous coal particles explode during devolatilization? Additional analysis and experiments will be conducted to answer these questions and develop a new large particle oxidation submodel.

Advanced Fixed-Bed Model Development and Evaluation (BYU) - The objectives of this task are to develop an advanced fixed-bed model incorporating the advanced submodels for large particle devolatilization and large particle oxidation and gasification, and to evaluate the model by comparing its predictions with the experimental data available from the literature. Advanced fixed-bed gasifiers are an integral part of the U.S. Clean Coal Technology (CCT) program and have been considered for integrated gasification combined cycle (IGCC) power generation systems and for mild gasification of lump coal. Recently, novel configurations have been proposed for gasification of caking coals and for mild gasification of lump coal. These configurations include the staged PyGas gasifier of the Gasification Product Improvement Facility (GPIF) project (Brown and Sadowski, 1991), and rotary kiln gasifier of the ENCOAL project (USDOE, 1993). Most of the available fixed-bed models can simulate only traditional fixed beds and there is a need to develop an advanced fixed-bed model capable of simulating both the traditional and emerging, novel gasifiers.

In a previous DOE-METC project, a one-dimensional model for fixed-bed combustion and gasification of coal, FBED-1, was developed (Radulovic et al., 1994). The FBED-1 model has achieved major advances in the treatment of various chemical and physical processes as well as in the solution procedure and has been extensively evaluated. There are still several important issues which must be resolved in the development of an advanced fixed-bed model capable of providing realistic simulations of the emerging configurations. These issues include treatment of large particle devolatilization processes, large particle gasification and oxidation processes, development of robust numerical solution methods, treatment of multiple additions and withdrawals of gases, handling of different flow patterns such as cocurrent, crosscurrent and countercurrent, and evaluation of the advanced model. The FBED-1 model provides a solid foundation for further developments which are continuing in this laboratory.

In order to simulate the combined-bed gasifiers, a preliminary integration of the cocurrent flow option was implemented in the FBED-1 model. The modified code was successfully used to simulate the PyGas gasifier of the GPIF project. The pyrolyzer section was simulated using the zero-dimensional submodel, FBED-0. The freeboard section was simulated by assuming full chemical and thermal equilibrium for the gas phase and no heat and mass transfer between the gas and solid phases. Both the upper and the lower fixed beds were simulated using the modified, fixed-bed model. The detailed profiles for the countercurrent and cocurrent sections of the gasifier are shown in Figure 4. The results predicted about 10% conversion of feed coal in the cocurrent section of the gasifier. Char consumption is due to gasification by CO_2 and H_2O. The gasification rates are higher at the top of the cocurrent section where temperature is relatively high. These rates decay as the solids cool down due to the endothermic gasification reactions. H_2O shows considerable depletion whereas the amounts of CO_2 remain almost constant. Only small amounts of CH_4 are produced in this section. The amounts of CH_4 produced in the countercurrent section are slightly larger. Large amounts of CO and H_2 are produced in the countercurrent section. The peak solid temperature is about 1500 K which is desirable for dry-ash gasifiers such as the PyGas staged gasifier. The product gas, which is the mixed stream from the cocurrent and countercurrent sections, is rich in CO and H_2, and has small amounts of CH_4.

Additional improvements will be made in the FBED-1 model to make it a design and analysis tool of significant industrial utility. These improvements will include incorporation of a large particle devolatilization submodel and a large particle oxidation submodel being developed under this project. A robust solution method suitable for stiff, non-linear problem of fixed-bed systems will be implemented. The model will be evaluated by comparison with the experimental data.

Submodel for Lean Premixed Combustion of Natural Gas in Industrial Gas Turbines (BYU) - A submodel for lean, premixed combustion (LPC) of natural gas in industrial gas turbines is being developed and implemented in a model being developed under independent funding for practical combustors. The submodel must incorporate finite-rate chemistry and predict NO_x and CO emissions at conditions approaching blowout (0.5 to 0.6 stoichiometric ratio in the primary zone). Proper accounting of the effects of chemistry/turbulence interactions is important. The Monte Carlo pdf method (Pope, 1985) is being considered as a basis for the submodel. A partially-stirred reactor (PaSR) model is being used to investigate the Monte Carlo pdf method. The PaSR (Chen, 1993) is similar to the perfectly stirred reactor (PSR) model, with no spatial variation of mean fluid properties. The difference

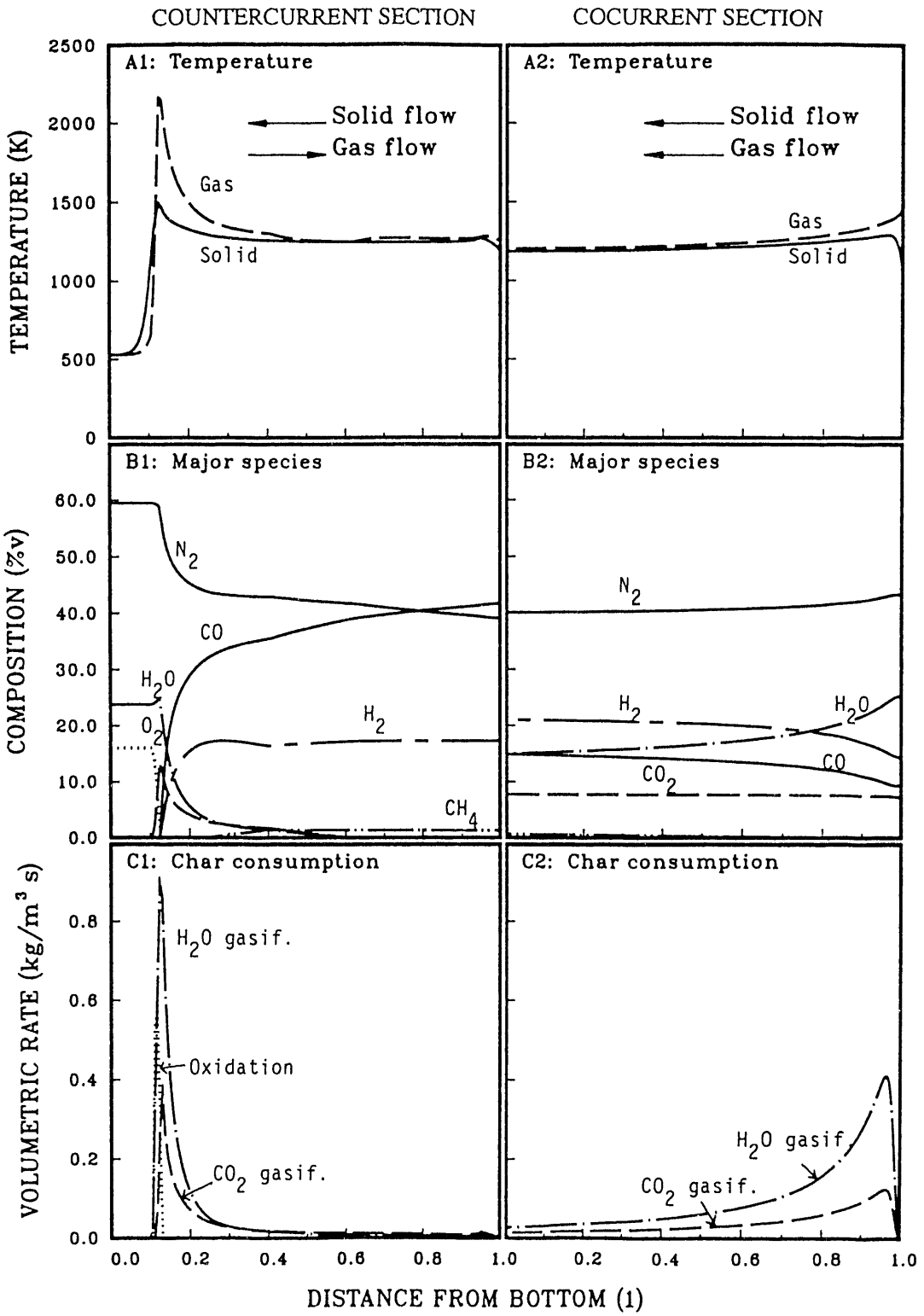

Figure 4. FBED-1 Predictions for the Countercurrent and Cocurrent Sections of the Staged PyGas Gasifier

is that molecular mixing is incomplete, so that the reactive fluids are not completely diffused into one another. Hence, there is a finite rate, given by a mixing frequency, at which the reactive fluids are mixed on a molecular level, as well as a finite rate at which they react after being mixed. Both the mixing and reaction time scales are important in the PaSR.

Calculations are being performed at conditions typical of LPC in stationary gas turbine combustors (premixed methane in air, 700 K inlet, 0.5~0.6 equivalence ratio, 15 atm, 10-20 ms residence time, and 100-5000 s^{-1} mixing frequency). The PaSR is being studied for several reasons. First, it provides an opportunity to understand the Monte Carlo pdf method in a simple model framework without the added complexities of fluid dynamics calculations. Second, many of the subroutines in the PaSR code may be applicable to a pdf submodel in PCGC-3 with little or no modification. Third, the PaSR model is a viable engineering model in its own right, with capability for including full chemistry (critical for predicting trace species). Fourth, the lessons learned from the PaSR are directly relevant to pdf methods for multi-dimensional flow, since the pdf equation for the PaSR is a degenerate case (integrated over reactor volume) of the pdf for the multi-dimensional case. Fifth, the PaSR provides an alternate test bed (to the more commonly used stirred-tank and plug-flow models) for evaluating reduced chemical schemes. And sixth, the PaSR provides a test bed for mixing models, a critical element of pdf models, in the context of full kinetics.

Results have been obtained using a reduced Miller-Bowman scheme (without C_2 chemistry and prompt NO) (Correa and Braaten, 1993). The effects of mixing rate, pressure, and mixing model were investigated. The effects of mixing rate at 15 atm and using the modified Curl's mixing model (Chen, 1993) are shown in Fig. 5. The importance of in-combustor mixing, even for premixed reactants, is clearly shown. Mixing of hot, partially-reacted particles in the combustor with the cold, incoming particles, is necessary to sustain combustion. Stable combustion was not achievable with a mixing frequency of 300 s^{-1} and lower. As shown in the figure, the PaSR converged to the non-reacting state at a mixing frequency of 300 s^{-1}. The higher the mixing frequency, the higher the temperature and the more complete the combustion, as the cold particles are quickly heated and brought to reaction temperature. The stochastic steady state is reached more rapidly with more rapid mixing. CO and the heat release chemistry (i.e. temperature) converge to the stochastic steady state at about the same rate, while NO converges considerably more slowly. This observation is in agreement with that of Correa and Braaten (1993). Scatter plots and pdf plots (not shown here) showed that the particles became more uniform in their properties as mixing frequency increased.

The above results were obtained with the modified Curl mixing model (Chen, 1993). The effect of the mixing model was investigated by repeating the calculations for a mixing frequency of 1000 s^{-1} with the Interaction-by-Exchange-with-the-Mean (IEM) model, but the solution converged to the non-reacting case. It was therefore decided to reproduce the results of Correa (1993) for CO/H_2/air combustion with a goal of determining whether the IEM model is implemented correctly in the PASR code. These calculations are in progress. If successful, calculations will then be performed with a full kinetic scheme for natural gas combustion, with a view toward obtaining a suitable reduced mechanism for use in a submodel to be implemented in a 3-D gaseous combustion code for application to lean, pre-mixed gas turbines.

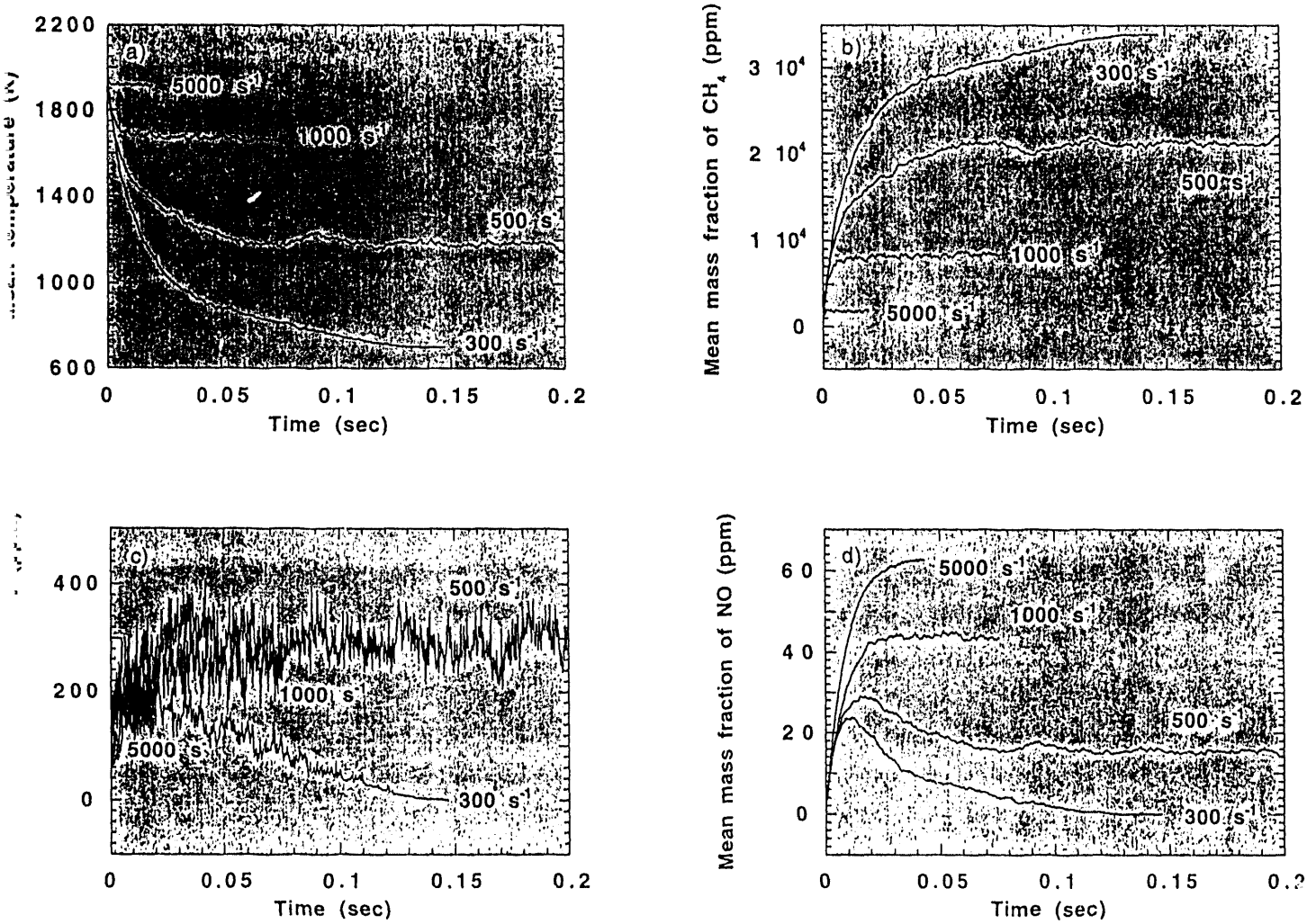

Figure 5. PaSR Predictions for Fuel-Lean, Premixed Methane Combustion in Air (0.6 Equivalence Ratio, 15 atm, 700 K Inlet, 10 ms Residence Time

FUTURE WORK

Work during the next year will include: 1) completion of simplified FG-DVC models for fixed-beds and fluidized-bed reactors; 2) integration of a particle heat transfer model with a simplified FG-DVC model; 3) complete stochastic particle dispersion model; 4) complete formulation of transport reactor code; 5) complete integration of simplified FG-DVC model into fluidized-bed code; 6) complete formulation of a large particle oxidation model; 7) complete integration of a large particle devolatilization submodel (based on FG-DVC) into FBED-1; 8) implement improved numerical solution method for FBED-1; 9) extend the PaSR pdf model to the case of natural gas combustion and use the model to develop/evaluate a suitably reduced kinetic mechanism for application in multi-dimensional flame codes.

REFERENCES

Bateman, K. J., Germane, G. J., Smoot, L. D., "A High Pressure Facility for Measurement of Oxidation Rates of Mm-Sized Chars," in preparation, Fuel (1994a).

Bateman, K. J., Germane, G. J., Smoot, L. D., and Blackham, A. U., "Effect of Pressure on Oxidation Rates of Mm-sized Char," in review, Fuel (1994b).

Brown, M.J., and Sadowski, R.S., "The PyGas Process, as Modeled by DOE-MGAS & KRW Kinetic Rate Equations," paper presented at the International Power Generation Conference, San Diego, CA, (October 1991).

Chen, J. -Y., "Stochastic Modeling of Partially Stirred Reactors," Fall Meeting of the Western States Sections/The Combustion Institute, Paper no. 93-071 (1993).

Correa, S. M., "Turbulence-Chemistry Interactions in the Intermediate Regime of Premixed Combustion," Comb. Flame, 93: 41-60 (1993).

Correa, S. M., and Braaten, M. E. "Parallel Simulations of Partially Stirred Methane Combustion," Comb. Flam, 94: 469-486 (1993).

Gosman, A.D., and Ioannides, E., AIAA Paper, No. 81-0323 (1981).

Jakob, M., Heat Transfer, John Wiley and Sons, New York (1959).

Kloeden, P.E., and Platen, E., Numerical Solutions of Stochastic Differential Equations, Springer-Verlag, (1992).

Merrick, D., Fuel, 63, 540 (1983).

Pope, S. B., "PDF Methods in Turbulent Reactive Flows," Prog. Energy Combust. Sci, 11: 119-192 (1985).

Radulovic, P.T., Ghani, M.U., and Smoot, L.D., "An Improved Model for Fixed-Bed Coal Combustion and Gasification," in press, Fuel, (1994).

Shuen, J-S., Chen, L-D., and Faeth, G.M., AIChE J., 29, 167 (1983).

Synder, W.H., and Lumley, J.L., J. Fluid Mech., 48, 41 (1971).

U.S. Department of Energy, "DOE, Clean Coal Technology Demonstration Program: Program Update 1992 (As of December 31, 1992)," U.S. Department of Energy Report, Washington, DC, DOE/FE-0272 (1993).

Wang, L.-P., Stock, D.E., J. Fluid Eng., Trans. ASME, 114, 101 (1992).